LANGMUIR Article
Cite This: Langmuir 2019, 35, 12858−12875
pubs.acs.org/Langmuir

Simulation of Drop-Size Distribution During Dropwise and Jumping Drop Condensation on a Vertical Surface: Implications for Heat Transfer Modeling

Kimberly A. Stevens, Julie Crockett, Daniel Maynes, and Brian D. Iverson*

Department of Mechanical Engineering, Brigham Young University, 350 Engineering Building, Provo, Utah 84602, United States

ABSTRACT: Accurate models for condensation heat transfer are necessary to improve condenser design. Drop-size distribution is an important aspect of heat transfer modeling that is difficult to measure for small drop sizes. The present work uses a numerical simulation of condensation which incorporates the possibility of coalescence and coalescence-induced jumping over a range of drop sizes. Results of the simulation are compared with previous theoretical models and the impact of the assumptions used in those models is explored. In particular, previous drop-size distribution models may predict heat transfer rates less accurately for high contact angles and for coalescence-induced jumping since coalescence occurs over a range of drop sizes and does not always result in departure. The influence of various input parameters (nucleation site distribution approach, nucleation site density, contact angle, maximum drop size, heat transfer modeling to individual drops, and minimum jumping size) on the drop-size distribution and overall heat transfer rate is explored. Assignment of the nucleation site spatial distribution and heat transfer model affect both the drop-size distribution and predicted overall heat transfer rate. Results from the simulation suggest that, when the contact angle is large (as on superhydrophobic surfaces) and no coalescence-induced jumping occurs, the heat transfer may not be as sensitive to the maximum drop-size as previously supposed. Furthermore, this work suggests that when coalescence-induced jumping occurs, reducing the maximum drop size may not always increase heat transfer since drops similar in size to those removed by coalescence-induced jumping can contribute significantly to the overall heat transfer rate.

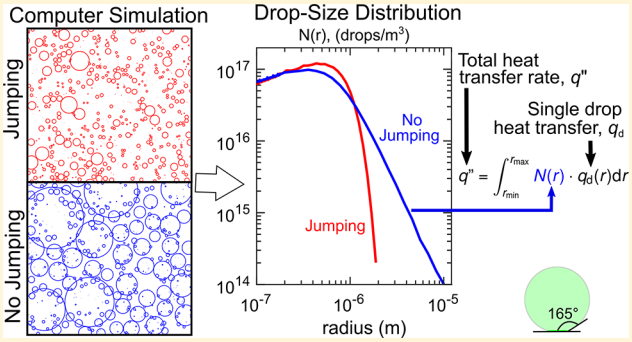

INTRODUCTION

Condensation has application in a range of industries including water desalination and harvesting,[1−3] energy conversion,[4−6] electronics cooling,[7] and environmental control.[8] Since it was discovered that heat transfer rates for dropwise condensation could be several times higher than film-wise condensation in the 1930s, much work has been done to model the heat transfer rate during dropwise condensation.[5,9−18] The modeling approach typically consists of expressions for the heat transfer rate to an individual drop (q_d) multiplied by the drop-size distribution (N). This product is then integrated over the range of drop sizes, as found on the condensing surface, to obtain the total heat transfer rate.[10−13]

$$q'' = \int_{r_{min}}^{r_{max}} N(r) q_d(r)\, dr \tag{1}$$

The individual drop heat transfer rate and the drop-size distribution are of equal importance in determining the overall heat flux to the surface, q'', during condensation. Therefore, developing an accurate expression for the drop-size distribution is an integral part of modeling the overall heat transfer rate during dropwise and jumping drop condensation and is the focus of this work.

One of the earliest and most adopted approaches to modeling the condensation heat transfer rate came from Le Fevre and Rose in 1966.[11,19] This work included both a semiempirically derived expression for the drop-size distribution as well as a model for heat transfer to an individual drop. The drop-size distribution was of the form

$$N(r) = \frac{1}{3\pi r^2 \hat{r}} \left(\frac{r}{\hat{r}}\right)^{-2/3} \tag{2}$$

where $\hat{r}$ is the average maximum radius of the drops, or the average size to which drops grow before gravity-induced shedding. N is the drop-size distribution in drops/m^2/m and described in further detail in the Methods section of this text. Other theoretical models agree well with the Le Fevre and Rose model.[19−21] The power law expression in Le Fevre and Rose's model has been experimentally validated for distributions in the range $r > 5 \times 10^{-5}$ m, but drop-size distributions for smaller drop sizes have not been reported due to the difficulty of imaging these drops.[10,19,22,23] Further, in reports

Received: July 18, 2019
Revised: September 9, 2019
Published: September 11, 2019

DOI: 10.1021/acs.langmuir.9b02232
Langmuir 2019, 35, 12858−12875

that do include drop size measurements in the range 5×10^{-5} m $< r < 5 \times 10^{-4}$ m, the distribution function resolution is coarse.

In 1975 Tanaka observed, by means of population balance theory, that drop growth during condensation could be separated into two regimes: growth dominated by direct condensation and growth dominated by coalescence with neighboring drops.[21] He observed that the distribution function for larger drops follows a power law relationship, as predicted by Le Fevre and Rose,[11,19] but that the distribution function for smaller drops would be significantly different. In 2011, building on the work of Tanaka and others,[24−26] Kim and Kim[12] used population balance modeling to develop a distribution function and heat transfer model for drops with contact angles greater than 90°. They showed that the distribution function was dependent on both the solid−liquid contact angle of the condensing drops and the nucleation site density on the surface. Miljkovic et al.[13] extended the work of Kim and Kim[12] to model drops on superhydrophobic surfaces. Superhydrophobic surfaces combine surface roughness with hydrophobic chemistry to achieve high solid−liquid contact angles (>145°) and high drop mobility (sliding angles <10°).[27,28]

Condensing drops on superhydrophobic surfaces have been shown to adopt various wetting states, depending on the surface subcooling and properties (particularly the relationship between the nucleation site density and surface feature density).[29,30] Superhydrophobic surfaces can be designed such that surface adhesion forces are low enough that the energy released upon coalescence of condensing drops can propel the drops away from the surface.[14,31−34] When the surface is oriented vertically, coalescence-induced jumping can lead to permanent departure of the drops from the surface. The heat transfer model proposed by Miljkovic et al.[13] accounted for additional thermal resistance due to surface roughness, various possible wetting states of condensing drops, and the possibility for coalescence-induced jumping thereby providing a framework for modeling condensation heat transfer on superhydrophobic surfaces.

Previous models offer valuable insight regarding the distribution in the direct-condensation-dominated growth regime,[12,13,21,24−26] but the lack of existing experimental drop-size distribution measurements for smaller drops has precluded validation. Since smaller drops account for the majority of the heat transfer that occurs during condensation, it is essential to obtain accurate distribution functions in this range. Solution of the differential equation resulting from population balance modeling requires the assumption of an instantaneous, rather than gradual transition between direct-condensation-dominated growth and coalescence-dominated growth. Though small droplet growth may be dominated by direct condensation, coalescence can occur over a range of drop sizes and therefore can influence the distribution at smaller sizes than the instantaneous transition point used by previous models. Another difficulty with population balance modeling occurs when coalescence-induced jumping is present. On realistic surfaces, jumping occurs for only a portion of the coalescence events that occur. However, when Miljkovic et al.[13] used population balance modeling to predict the distribution function on surfaces with jumping, of necessity they assumed all coalescence events result in jumping and that all coalescence events occur at a single size. Models derived using population balance theory are fundamentally limited by their inability both to address coalescence in the direct-condensation-dominated growth regime and to handle coalescence-induced jumping over a range of sizes. Zhang et al. proposed a theoretical model to account for coalescence over a range of drop sizes, but they only considered the case where jumping occurs, and they assumed that most coalescence events result in departure (limiting the applicability of the model to condensation on vertical surfaces with high contact angles and low adhesion).[35]

In contrast to population balance modeling, other researchers have used computational modeling to gain insight into condensation behavior on superhydrophobic surfaces and to validate previously proposed theoretical models. Gose et al.[36] and Tanasawa and Tachibana[20] were among the first to attempt to use computer models but, due to limitations in computing power, only investigated low distribution densities. Glicksman and Hunt[37] obtained distribution functions with a simulation that showed good agreement with the Le Fevre and Rose[11] distribution function at larger drop sizes and diverged at smaller sizes, based on the nucleation site density. However, their simulation was limited to drops with a contact angle of 90° and did not incorporate gravity-induced sweeping of drops. Mei et al. used a computer simulation to obtain the drop distribution also for a contact angle of 90°, but their results were intended for larger drop sizes where the distribution function was already well established.[38] Barati et al. used a numerical simulation of dropwise condensation to investigate condensation as a function of time for drops with a contact angle of 88°, though they did not report steady state drop distribution data.[39] Meng et al. demonstrated how a computer simulation could incorporate the possibility of coalescence-induced jumping but did not use their model to obtain an expression for the drop-size distribution and focused on predicting heat transfer for drops with a single contact angle (140°) and maximum drop size (30 μm).[40] Birbarah et al. used numerical simulations to predict drop-size distributions, though their analysis focused on the case when coalescence-induced jumping occurs.[41] Others have used numerical simulations to gain insight into various aspects of condensation and vapor deposition behavior but have not focused on the steady state distribution function and predicted overall heat transfer rate.[42−47]

In summary, previous dropwise condensation modeling approaches have offered valuable insight regarding drop growth and condensation heat transfer rates. However, these previous approaches have been limited by their assumptions or application. Population balance modeling involves limiting assumptions regarding small drop coalescence. Previous computer simulations have included a limited scope of physical conditions and, with few exceptions, these simulations were not applied to predict steady-state drop-size distributions.

The present work reports a computational approach to obtain the steady state drop-size distribution and associated time-averaged heat transfer rates for dropwise condensation over a range of contact angles from 90 to 180°. Condensation is simulated in a Lagrangian approach, similar in form to previous computational approaches, allowing for coalescence at naturally occurring drop sizes.[20,36−47] Unlike previous computational simulations, the present work considers how the departure of drops both by jumping and gravity-induced sweeping influences the steady state drop-size distribution and associated time-averaged heat transfer rates. The present work spans also a larger range of physical conditions than previous

DOI: 10.1021/acs.langmuir.9b02232
Langmuir 2019, 35, 12858−12875

studies. The present work only considers flat or nanostructured surfaces without a microscale feature size. The impact of various input parameters (i.e., maximum drop size, contact angle, nucleation site selection method, and coalescence-induced jumping) on the distribution function and overall heat transfer rates is explored. Understanding the relative impact of these parameters on overall heat transfer rates is essential for the design of improved condensing surfaces. The main contributions of this work are 2-fold. First, a computational condensation simulation is used to explore how various assumptions and physical conditions influence the drop-size distribution and predicted heat transfer rate. Second, results suggest that when the contact angle is large and coalescence-induced jumping occurs previous models fail to accurately predict the relationship between maximum drop size and heat transfer rate, a relationship which is crucial to understand for designing improved condensing surfaces.

RESULTS AND DISCUSSION

Results are presented as follows. First, a description of a computer simulation for dropwise and jumping drop condensation is described in the sections titled Simulation Overview, Initial Nucleation, Individual Drop Growth, Drop Coalescence, Drop Sweeping, and Distribution of New Drops. These sections describe the methods and physics behind each aspect of the simulation approach. Second, the drop-size distributions obtained from the simulation are compared with other theoretical models as a form of validation (Model Validation and Comparison section) and to demonstrate the influence of previous assumptions. Third, the effects of assumptions regarding condensation behavior (i.e., individual drop heat transfer model, nucleation scheme), and different physical conditions (i.e., contact angle, maximum drop size, initial nucleation density, and minimum jumping size) are explored, providing insight regarding the influence of these input parameters and model accuracy. Understanding the influence of contact angle, maximum drop size, initial nucleation density, and minimum jumping size on overall heat transfer rates is important for improved surface design. Finally, the predicted influence of contact angle and maximum drop size on heat transfer rate is compared with that predicted using population balance modeling, indicating that population balance modeling may deviate from real behavior more significantly when the contact angle is large and coalescence-induced jumping occurs.

Simulation Overview. A computer simulation of dropwise condensation on a vertical, smooth hydrophobic, or nanostructured superhydrophobic surface is used to obtain insight regarding drop-size distributions and aggregate condensation heat transfer. The simulation is Lagrangian in nature, where individual drops are randomly distributed and their growth and interaction are governed according to physically based equations found in the condensation literature. The size and arrangement of the drops through time is used to obtain drop-size distributions and an overall heat transfer rate in a stochastic approach. At the beginning of the simulation, which is performed in MATLAB, drops are distributed on a surface at randomly selected nucleation sites, allowed to grow, coalesce, and depart either by sweeping or coalescence-induced jumping following the decision tree shown in Figure 1. At each time step, new drops are distributed. The simulation continues until a quasi-steady state condition is reached, as described in the Methods. Expressions for time-averaged drop-size distribution

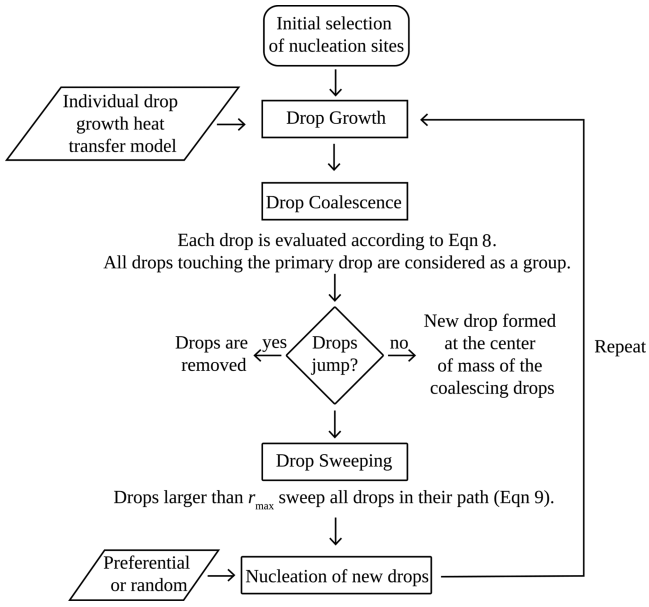

Figure 1. Overview of the steps in simulation of dropwise condensation on a vertical surface.

and overall heat transfer rates are obtained from the results of the simulation by counting the number of drops of a given size and tracking the heat transferred to individual drops throughout the simulation. The simulation assumes a constant contact angle during drop growth, negligible thermal resistance at the drop/surface interface, instantaneous sweeping and coalescence, that drops have a spherical-cap-shape, and that drops are in a suspended or partially wetting, mobile (subject to sweeping) state. The simulation considers condensation in a pure vapor environment in the absence of noncondensable gases. The following sections provide additional details about the modeling approach for each physical process, with more detailed descriptions and equations found in the Methods section.

Initial Nucleation. Prior to the start of the simulation, nucleation sites are randomly distributed across the surface with a user-specified nucleation site density (N_s). Though drops do not all spontaneously nucleate at the same instant, the approximation of simultaneous nucleation is used in the simulations to initialize the process. The simultaneous nucleation approximation at the onset of condensation is not expected to influence the steady state drop-size distribution since sweeping events repeatedly occur during steady state condensation, removing all drops on a portion of the surface, such that the influence of the initial distribution of drops becomes negligible over time. In fact, Leach et al.[42] found that the drop size distribution at long times was insensitive to initial conditions. Furthermore, other research works with similar computational approaches[20,36,37] have used the same assumption (see Introduction regarding computational approaches). A drop with radius r_{min} is placed at each site. Unless otherwise noted, r_{min} is equivalent to the smallest thermodynamically viable drop, r_{thermo}.

$$r_{thermo} = \frac{2T_{sat}\sigma}{h_{fg}\rho\Delta T} \tag{3}$$

where T_{sat}, σ, h_{fg}, ρ, and ΔT are the saturation temperature, surface tension, latent heat of vaporization, fluid density, and

DOI: 10.1021/acs.langmuir.9b02232
Langmuir 2019, 35, 12858−12875

difference between the saturation and substrate surface temperatures.[48] For select cases described later in the text, r_{min} can be larger than r_{thermo}.

Individual Drop Growth. At each time step of the simulation, drops grow according to a specified model for the heat transfer rate to a single drop, q_d. The influence of using different models on the heat transfer rate is compared in the section Influence of Heat Transfer Model. First, a thermal resistance model (implemented by Kim and Kim[12] and Miljkovic et al.[13]) is used. For a flat or nanostructured surface where the microscale feature height may be approximated as zero and droplet jumping does not occur, the Kim and Kim[12] and Miljkovic et al.[13] expressions for heat transfer to a single drop are identical. Second, Chavan et al.[49] solved for the heat transfer rate to drops growing by condensation with a constant contact angle in a two-dimensional numerical simulation and found significant differences from the thermal resistance approach, which requires the assumption that the drop surface temperature be isothermal. They reported a piece-wise expression for the Nusselt number as a function of the Biot number and advancing contact angle for drops between 100 nm and 2 mm, which will be referred to as the "Chavan model". Adhikari et al. recently proposed a finite element model covering a different range of Biot numbers than that covered by the Chavan model.[50] They provided tabulated data for the heat transfer rate to a single droplet as a function of Biot number and advancing contact angle. To avoid the computationally expensive task of repeatedly referring to the tabulated data to calculate the heat transfer rate, a polynomial fit to the log of the heat transfer rate as a function of radius for a given contact angle was used in the simulation and will be referred to as the "Adhikari model". The difference between the tabulated data and the polynomial was always less than 2%. Predictions of the individual drop heat transfer rate, q_d, derived from these models are shown in Figure 2 as a function of droplet radius. The Adhikari and Chavan models yield similar predictions of q_d except at small drop sizes. The heat transfer rate for the thermal resistance model approaches zero at the nucleation drop size and provides a lower prediction of the heat transfer rate at larger drop sizes relative to the computational models by Chavan and Adhikari.

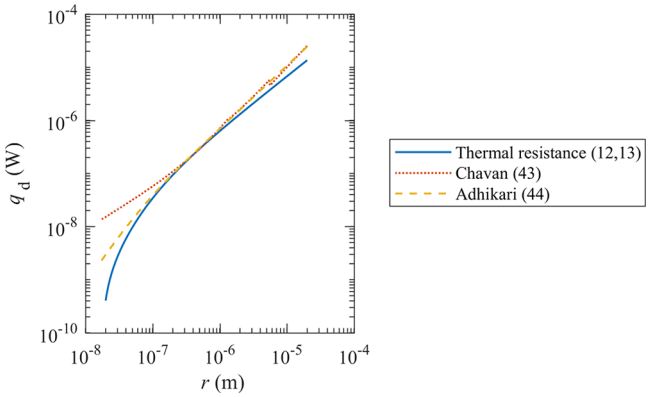

Figure 2. Comparison of models for the heat transfer rate to a single condensing drop, q_d, which are used in the simulation. The slight discontinuity observed in the Chavan model is a result of the piece-wise function provided for the Nusselt number in their work.

For each heat transfer model, the amount of energy transferred to each drop over a given time step is computed by multiplying the heat transfer rate to a single drop at the size corresponding to the previous time step with the time step, δt. This transferred energy results in droplet growth and the new drop volume is computed as

$$V_{new} = V_{old} + \frac{q_d(r)\delta t}{\rho h_{fg}} \tag{4}$$

where ρ and h_{fg} are the fluid density and latent heat of vaporization. Assuming a drop with a spherical cap, the corresponding drop radius can then be calculated as

$$r_{new} = \left(\frac{3V_{new}}{\pi(2 - 3\cos\theta + \cos^3\theta)} \right)^{1/3} \tag{5}$$

where θ is the solid−liquid contact angle. The spherical cap assumption is a good approximation for drops smaller than the capillary length, which prevails for the drops considered in the present work (and all condensing drops that are not in a highly pinned state prior to flooding).

Drop Coalescence. As drops grow from r_{min} they will eventually become large enough to touch other drops, as further described in the Methods section. When this occurs, they either are replaced by a new drop located at the center of mass of the parent drops with the same total volume, representing coalescence, or are removed from the surface, representing coalescence-induced jumping resulting in departure from the surface. Three options for addressing a coalescence event can be selected in the simulation and are included to investigate the effects of coalescence-induced jumping. The three options that result from coalescence include drops that will (1) always depart, (2) never depart, or (3) depart if at least two of the drops involved in the coalescence event are larger than a minimum threshold (specified by an input parameter to the simulation, r_j). Use of a minimum radius to determine whether coalescence results in jumping has physical rationale as researchers have observed that coalescence-induced jumping only occurs for drops larger than a minimum radius, and this radius is highly dependent on the surface structure.[33,34,51−53] For specially designed surfaces, drops as small as 500 nm have been shown to jump upon coalescence,[33,34,51] but for more common superhydrophobic surfaces, such as copper oxide, the minimum radius for jumping is typically on the order 10 μm. Recent research has shown that, in addition to minimum drop size, surface feature length scale, drop wetting state, relative size mismatch, and number of drops involved in a coalescence event all may influence whether or not a coalescence event will result in coalescence-induced jumping.[33,34,51−53] Though not considered here, these additional conditions could be incorporated into an energetic-based model for jumping.

Drop Sweeping. On a vertically oriented surface, when a drop grows to a sufficiently large size (r_{max}), the force of gravity will overcome the adhesive force and the drops will roll down the oriented surface, sweeping and removing all the drops in its path, as described in the Methods section. The maximum drop size, r_{max}, is specified for each simulation run. An expression to determine r_{max}, derived from a force balance between gravity and the adhesive force, has been used by other researchers to determine the maximum drop size.[12,13] However, these expressions include both the advancing and receding contact angles, necessitating a specification of two variables rather than one. Additionally, it has recently been shown that the adhesive

DOI: 10.1021/acs.langmuir.9b02232
Langmuir 2019, 35, 12858−12875

force can change depending on the degree of subcooling of the surface; this dependence has not yet been fully explored.[34,54,55] Therefore, in this work, r_{max} remains as a specified input parameter so that the resulting distribution functions are independent of subcooling and surface properties other than the contact angle and r_{max}.

Distribution of New Drops. At each time step, new drops are distributed either randomly or based on preferential nucleation sites coincident with the original nucleation locations. When drops are distributed randomly, the number of new drops is determined so the original nucleation site density, N_s, is maintained on the portion of the surface not covered by drops, as follows:

$$n_{new} = \left(N_s - \frac{n}{A}\right)(A - A_b) \tag{6}$$

where A is the total area of the domain, n is the number of drops on the surface, and n_{new} is the number of new drops added in that time step. A_b is the sum of the base area of all drops on the surface, $A_b = \sum_{i=1}^{n} \pi(r_i \cos\theta)^2$. "Assuming that the initial nucleation density is constant implies that the presence of condensing drops does not change the surface temperature sufficiently to change the nucleation site density, which would depend on the substrate material, substrate geometry, and heat transfer rate. When new drops are distributed based on "preferential nucleation site" locations, the original nucleation sites from the first time step become the starting point of all future drops. When original nucleation sites are exposed, new drops begin to grow at these same locations. Preferential nucleation sites can exist on real surfaces (including smooth hydrophobic surfaces) due to surface irregularities, nonhomogeneity in native surface chemistry, etc.[29,56,57] Furthermore, evidence suggests that drops may leave behind a small amount of liquid from which subsequent drops may grow.[58−62] However, it is also possible for new nucleation sites to appear, particularly if all of the preferential sites are covered by drops. It is expected that realistic nucleation behavior is best described by a combination of these two approaches.

Input Parameters and Operating Conditions. The following sections compare the drop-size distribution obtained using the simulation with prior modeling approaches and explores the influence of the implemented heat transfer model (thermal resistance, Chavan, or Adhikari), nucleation scheme (random or preferential), maximum drop size (r_{max}), contact angle (θ), initial nucleation site density (N_s), and jumping on the time-averaged distribution function, N, and spatially and time-averaged heat transfer rate, q''. These parameters (heat transfer model, nucleation scheme, maximum drop size, contact angle, initial nucleation density, and presence of jumping) are specified as input conditions for the simulation. In practice, maximum drop size, contact angle, initial nucleation density, and minimum jumping size depend on the condensing substrate physiochemical properties, surface texturing, and surface subcooling, and could be measured for a given surface and set of operating conditions.[37,47,63] All results presented are based on a saturation temperature, T_{sat} = 22 °C and $\Delta T = T_{sat} - T_s$ = 1 °C. Unless otherwise indicated, the simulations were run with an initial nucleation density $N_s = 1 \times 10^{11}$ drops/m^2, utilization of the Adhikari heat transfer model, no coalescence-induced jumping, and a random nucleation scheme. Since a nanostructured surface is assumed, a constant contact angle is used, as described in the Methods section, along with further description of the simulation details, such as time grid independence and domain size. The maximum drop size (radius) ranged from 2×10^{-5} to 2×10^{-4} m and the contact angle varied from 90 to 165°. For dropwise condensation on smooth, hydrophobic, vertically oriented surfaces, the maximum drop size is often considered to be on the order of the capillary length (2.7 mm for water), though considerably smaller maximum drop sizes (<0.1 mm) can be achieved on superhydrophobic surfaces with low contact angle hysteresis or in the presence of vapor shear, centrifugal forces, or wettability gradients.[10,17] However, for a nucleation density of 1×10^{11} drops/m^2, the drop size range, which is limited by the simulation domain size, was selected to allow for computationally reasonable simulations. Significantly larger drop (and domain) sizes could be explored at lower nucleation densities for similar computational cost.

Model Validation and Comparison. The drop-size distributions obtained from the simulation are compared with those predicted by previous investigators in order to validate the approach. Assumptions used by previous investigators are enforced in the simulation so that a comparison can be made. First the drop-size distributions for surfaces without coalescence-induced jumping are compared, and then drop-size distributions for surfaces with coalescence-induced jumping are compared. The reason for the differences caused by the enforcement and removal of the simplifying assumptions are discussed.

The models proposed by Kim and Kim[12] and Miljkovic et al.[13] both divide the distribution function into two drop growth regimes: (1) growth mainly by direct condensation and (2) growth primarily by coalescence. In these models, the region where drop growth is dominated by coalescence is modeled using the power law relation proposed by Le Fevre and Rose[11,19] in eq 2. Both works use population balance modeling to approximate the distribution function in the direct-condensation-dominated growth regime and solve the resulting differential equation with two boundary conditions at the transition between the two regimes (i.e., at the equilibrium radius, r_e). The first boundary condition stipulates that the distribution functions for the two regimes have the same value at r_e. The second boundary condition stipulates that the derivative of the natural log of the distribution functions also be equal

$$\frac{d}{d(\ln r)} \ln n(r) = \frac{d}{d(\ln r)} \ln N(r) = -\frac{8}{3} \tag{7}$$

where $n(r)$ and $N(r)$ are the distribution functions in the direct-condensation- and coalescence-dominated growth regimes, respectively. In the case where the surface texture height can be considered negligible and no jumping occurs, the only difference in the distribution functions proposed by Kim and Kim[12] and Miljkovic et al.[13] is the value of the equilibrium radius. Kim and Kim[12] calculate r_e as half of the average distance between drops, assuming the drops are arranged in a square lattice, or $r_e = 1/(2\sqrt{N_s})$. Miljkovic et al.[13] use half of the average distance between drops if the drops are distributed following a Poisson distribution, or $r_e = 1/(4\sqrt{N_s})$. A Poisson distribution has been shown to accurately reflect the distribution of drops during condensation on surfaces of nominally uniform wettability[29,30,56] and is the primary difference between the two previous works by Kim and Kim and Miljkovic et al. in the absence of a microstructure and

DOI: 10.1021/acs.langmuir.9b02232
Langmuir 2019, 35, 12858−12875

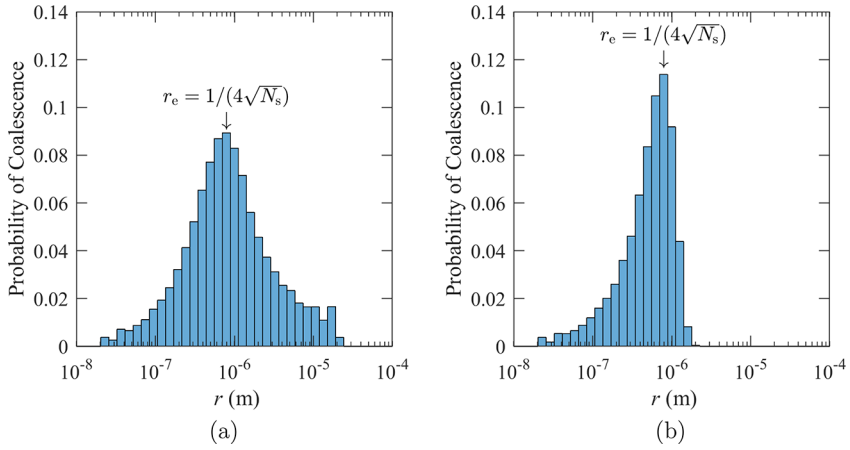

Figure 3. Probability coalescence will occur at a certain size. In the cases shown, nucleation sites are distributed following a Poisson distribution, the Adhikari individual drop heat transfer model is used, θ = 165°, and (a) coalescence does not result in departure or (b) coalescence always results in departure. The most common size for drop coalescence to occur is $r = 1/(4\sqrt{N_s})$, but coalescence occurs over a wide range of drop sizes. When drops remain on the surface following coalescence they continue to coalesce until r_{max}. However, when coalescence results in departure, drops do not grow large enough to reach r_{max}, and the coalescence-size distribution drops off sharply.

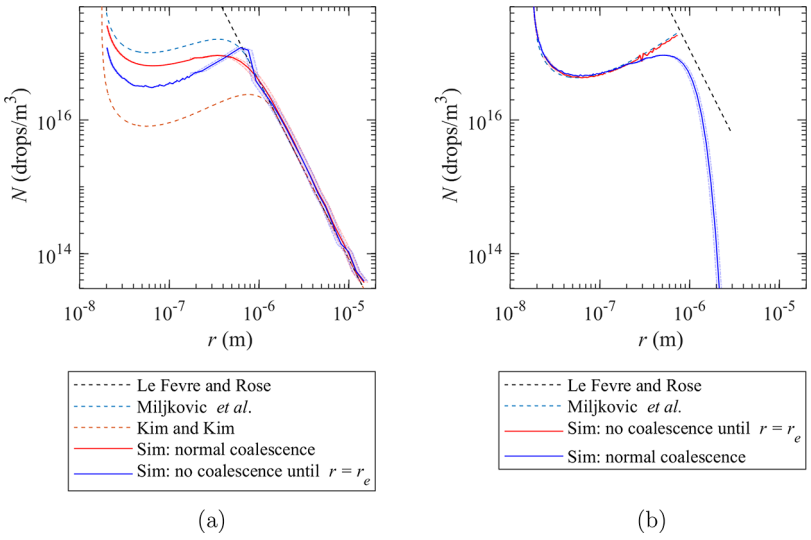

Figure 4. (a) Comparison of the distribution functions obtained from simulation (red) with those proposed by Kim and Kim,[12] Miljkovic et al.,[13] and Le Fevre and Rose.[11,19] The light shading represents the uncertainty associated with creation of the distribution, as described in the Methods section entitled, Obtaining the Drop-Size Distribution. When coalescence is not suppressed the distribution (red) converges with the Le Fevre and Rose distribution at a size larger than that proposed by Miljkovic et al. and smaller than that proposed by Kim and Kim. When coalescence is suppressed until $r = 1/(4\sqrt{N_s})$ the simulated distribution (blue) matches the distribution proposed by Miljkovic et al. at $r = r_e$, but the slope of the distribution function is discontinuous. (b) Drop-size distribution functions for which all coalescing drops either jump (red) or for which coalescence is suppressed and all drops depart at $r = 1/(4\sqrt{N_s})$ (blue). The noncoalescing case agrees well with the distribution proposed by Miljkovic et al. for suspended drops with $r_{max} = 1/(4\sqrt{N_s})$ (dashed blue). The difference between the simulated distributions demonstrates the influence of assuming coalescence occurs at a single drop size. The Le Fevre and Rose distribution for $r_{max} = 1/(4\sqrt{N_s})$ is also shown (dashed black). All other distributions shown in (a) and (b) correspond to the case where θ = 165°, $r_{max} = 2 \times 10^{-5}$ m, and $N_s = 1 \times 10^{11}$ drops/m^2.

coalescence-induced jumping. The separation of the distribution function into two separate regimes facilitates the use of population balance modeling and allows solution of the accompanying differential equation. However, in reality the onset of coalescence is not expected to occur at a single size; drops grow by direct condensation throughout their lifetime, and coalescence does not suddenly occur at a single size. If one were to plot a histogram of drop sizes at coalescence on a surface with nucleation sites following a Poisson distribution, coalescence would most frequently occur at $r = 1/(4\sqrt{N_s})$, but coalescence would occur over a range of drop sizes, as observed during condensation and illustrated in Figure 3. Figure 3 was generated by counting the size of all drops involved in coalescence during simulation of two scenarios: first, where coalescence does not result in departure, and second, where coalescence always results in departure.

In order to compare the results from the current simulation approach with the distribution functions proposed by Kim and Kim[12] and Miljkovic et al.,[13] one scenario considered suppressed coalescence until $r = r_e$ since no coalescence prior to $r = r_e$ is assumed in their models. In this comparison case, the thermal resistance heat transfer model was used, θ =

DOI: 10.1021/acs.langmuir.9b02232
Langmuir 2019, 35, 12858−12875

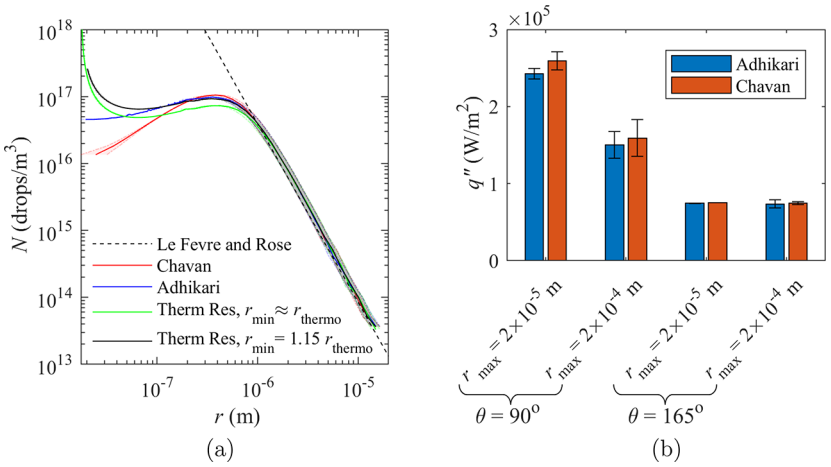

Figure 5. (a) Drop distribution functions obtained using three different models for heat transfer to a single drop. Two different r_{min} are used for the thermal resistance model. In the case labeled $r_{min} \approx r_{thermo}$, r_{min} is 1×10^{-13}% larger than r_{thermo}. The contact angle for the distributions shown was 165° with $r_{max} = 2 \times 10^{-5}$ m. The heat transfer model has a significant influence on the distribution functions at small radii. (b) Time-averaged rates of heat transfer for the two models derived from numerical simulations. The influence of heat transfer model on the overall heat transfer rate becomes less significant when the contact angle is large.

165°, $r_{max} = 2 \times 10^{-5}$ m, and $N_s = 1 \times 10^{11}$. Unsurprisingly, suppressing coalescence results in a function that has a discontinuous first derivative at $r = r_e$, as shown in blue in Figure 4a. Note that in all plots of the drop-size distribution obtained from simulation, light shading represents the uncertainty associated with creation of the distribution, as described in the Methods section entitled, Obtaining the Drop-Size Distribution. At $r > r_e$, the simulation distribution matches the distribution predicted by Le Fevre and Rose[11,19] and Miljkovic et al.[14] When suppressing coalescence, the distribution predicted by the simulation satisfies the first boundary condition used to solve the population balance modeling differential equation at $r = 1/(4\sqrt{N_s})$, confirming that is an appropriate boundary condition for randomly distributed nucleation sites when coalescence is suppressed. However, for $r < r_e$ the distribution is significantly lower than that predicted by Miljkovic et al.[13] The Kim and Kim[12] and Miljkovic et al.[13] models do not have a discontinuous slope at $r > r_e$ since the second boundary condition forces the slope at $r = r_e$ to match that of the Le Fevre and Rose[11] distribution. The only difference between Kim and Kim[12] and Miljkovic et al.[13] models in the absence of a microstructure is the assumption of a random or square lattice distribution of nucleation sites.

A second simulation scenario was considered where coalescence was not suppressed, but allowed to occur naturally (red distribution in Figure 4a). For this scenario, the distribution converges with the Le Fevre and Rose distribution for coalescence-dominated growth, and both boundary conditions are satisfied, as illustrated in Figure 4. The shape of the distribution function when coalescence is not suppressed is similar to those proposed by Kim and Kim[12] and Miljkovic et al.[14] However, rather than converging at $r = 1/(4\sqrt{N_s})$ or $r = 1/(2\sqrt{N_s})$, for this scenario the radius of convergence is observed to be somewhere in between, at approximately $r = 1 \times 10^{-6}$ m. The distribution function converges at a larger radius since coalescence occurs for drops with $r < 1/(4\sqrt{N_s})$. Coalescence of the drops causes the distribution function to decrease, thereby converging with the power law function at a larger radius. The similarity in shape between the distribution from simulation and the previous models provides confidence in the current approach. The difference in the radii of convergence with the Le Fevre and Rose distribution function arises from allowing coalescence to occur naturally, rather than at a single radii as modeled in population balance theory. Results from the simulation suggest that the distribution function in the direct-condensation-dominated regime converges with the power law function at a larger radius than $1/(4\sqrt{N_s})$, even though $r = 1/(4\sqrt{N_s})$ is the most common size for coalescence.

Miljkovic et al.[13] also modeled the distribution function for drops that depart via coalescence-induced jumping and assumed that drops would coalescence and depart when $r = r_e = 1/(4\sqrt{N_s})$, as shown in Figure 4b. For comparison, results from a third simulation scenario are shown where the coalescence was suppressed and all drops were removed from the simulation at $r = 1/(4\sqrt{N_s})$. Agreement between the distribution proposed by Miljkovic et al.[13] and this simulated distribution is good (less than 8% difference in predicted heat transfer rate), providing confidence in the results from simulation. The distribution function is also shown for a fourth scenario where coalescence is allowed to occur naturally and all drops depart upon coalescence. Drop coalescence causes a decrease in the distribution function relative to the case where coalescence is suppressed, and the distribution curve drops off gradually, rather than terminating immediately. Comparison of the two different distribution functions highlights the influence of suppressing coalescence on the distribution function. In all subsequent simulations described in this work, coalescence is not suppressed and is allowed to occur naturally. Since the drop-size distributions predicted by the simulation and Miljkovic et al.[13] agree when coalescence is suppressed and differ when allowed to occur naturally, the differences between results predicted by the simulation and those predicted by Miljkovic et al.[13] in Figure 4 can be assumed to arise from the assumption of suppressed coalescence employed by Miljkovic et al.[13]

The drop size distribution does not always monotonically decrease, as predicted by Le Fevre and Rose.[11,19] The Kim and Kim[12] and Miljkovic et al.[13] models as well as the current

DOI: 10.1021/acs.langmuir.9b02232
Langmuir 2019, 35, 12858−12875

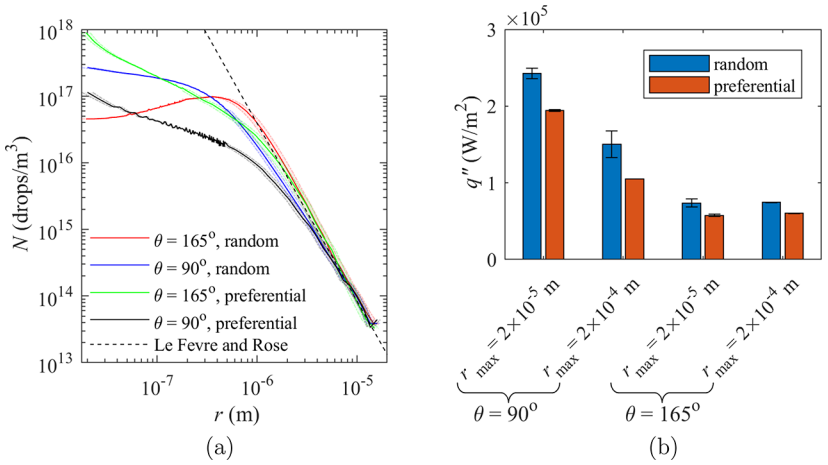

Figure 6. (a) Distribution functions for random and preferential nucleation schemes using the Adhikari heat transfer model for simulations with $N_s = 1 \times 10^{11}$ drops/m^2 and $r_{max} = 2 \times 10^{-5}$ m. (b) Time-averaged rates of heat transfer for the different nucleation schemes. A higher heat transfer rate is predicted when using the random nucleation scheme despite the fact that more small drops are predicted with the random nucleation scheme when the contact angle is large.

simulation all predict the existence of a local minimum for certain cases, as shown in Figure 4. Miljkovic et al. explain that the local minimum exists since the droplet growth rate is influenced by both the curvature resistance (which increases with decreasing radius) and conduction thermal resistance (which increases with increasing radius); the drop-size distribution increases for drops larger than the local minimum due to conservation of drops entering and leaving a drop population.[13] Additionally, a local minimum could also result from the nonuniform distribution of coalescence sizes. For example, consider a bin of condensing drops spanning the range $r = a$ to $r = b$, where r is the radius and $a < b$. Over time, drops which enter this range as they grow due to direct condensation will also leave the range by the same mechanism if they do not coalesce. As drops within this size range coalesce, they also leave the bin associated with this range. Drops will also enter the range as the result of coalescence of drops which are smaller than the range a to b. The net effect of drops entering and exiting via coalescence can also cause the drop-size distribution to increase or decrease with radius. If the size distribution of coalescence events is constant (i.e., drops were just as likely to coalesce at $r = 5 \times 10^{-8}$ m as at $r = 1 \times 10^{-6}$ m), then the drop-size distribution would monotonically decrease since coalescence results in two drops exiting a bin size and only one drop entering a bin size. However, the probability for coalescence at a particular size has a nonconstant distribution, as illustrated in Figure 3. When the drop-size distribution increases with increasing drop size, the net flux of coalescing drops (number of drops that enter minus the number exiting the range a to b) is positive, meaning that more drops have entered than left. A local minimum will not always exist in the drop-size distribution but will occur when the net flux of coalescing drops is positive.

Influence of the Heat Transfer Model. Three different models for heat transfer to an individual drop were used in the simulation to explore how they influenced the drop-size distribution and total heat transfer rate. The model selected for heat transfer to each individual drop influences the resulting distribution function. Drop-size distributions obtained using the three heat transfer models are compared in Figure 5a relative to the distribution predicted by Le Fevre and Rose.[11,19] The shape of the distribution is similar for all three models, though there are significant differences observed as the distribution departs from the power law function. In the thermal resistance model for $r = r_{thermo}$, the heat transfer rate is zero and drops will never grow. Therefore, r_{min} (smallest drop in the simulation) is chosen to be larger than r_{thermo} (smallest thermodynamically viable drop). To demonstrate the influence of increasing r_{min}, the distribution function for two different r_{min} values are shown: $r_{min} \approx r_{thermo}$ (r_{min} is 1×10^{-13}% larger than r_{thermo}) and $r_{min} = 1.15 r_{thermo}$. The first r_{min} was selected based on the numerical accuracy of the simulation. The second r_{min} was chosen at a point where the distribution function was no longer changing significantly with r_{min}. The distribution produced with the second r_{min} is likely more accurate since it agrees better with distributions produced using the Chavan and Adhikari models which do not assume an isothermal surface.

The Adhikari model was developed from simulations using Biot numbers in the range $0.0001 < Bi < 1000$, while the Chavan model was developed from simulations covering a larger range, $0.1 < Bi < 1 \times 10^5$. In the range of Biot numbers where the simulations overlap, the agreement between the simulations is good (better than 20%); however, for smaller drop sizes, the heat transfer rate (Figure 2) and distribution functions (Figure 5a), diverge (up to a factor of 5 for the individual drop heat transfer rate). The range of Biot numbers in the present work is $0.0064 < Bi < 284$. Therefore, it is assumed the Adhikari model is more appropriate. The time-averaged heat transfer rate for the Chavan and Adhikari models is presented in Figure 5b. The Chavan model predicts a higher heat transfer rate for smaller drops (see Figure 2) since drops of this size are outside of the range of Biot numbers predicted by their model and is reflected in the higher overall heat transfer rate predicted by the simulation. The heat transfer model makes a larger difference on the overall heat transfer rate when the contact angle is low, but the difference is considerably smaller for large contact angles.

The difference in the distribution function and heat transfer rate between the various models highlights the fact that the accuracy of the distribution function is dependent on the accuracy of the model for heat transfer to a single drop. Recently Xu et al. proposed a detailed model which includes two-dimensional conduction, convection in the drop, moving

DOI: 10.1021/acs.langmuir.9b02232
Langmuir 2019, 35, 12858−12875

contact line, mass transfer into the droplet, and interface expansion.[64] These authors did not provide an expression for the heat transfer rate to an individual drop, which precludes its application in the present work, but did suggest that current models which only consider conduction within the drop severely underestimate the heat transfer rate in larger drops. If the output of their model were to be combined with a more detailed distribution function, presumably a more accurate model for the overall heat transfer rate during condensation could be obtained.

Influence of the Nucleation Scheme. On a real condensing surface, nucleation sites typically occur at non-homogeneous defects on a surface and may be modeled as occurring randomly on a surface of uniform wettability. However, a drop removed (by sweeping, jumping, or coalescence) from the surface often leaves behind a portion of condensed liquid which serves as a nucleation site for future drops. Thus, in reality, the distribution of new nucleation sites may be expected to behave somewhere between the random and preferential approaches described above. The influence of selecting randomly distributed or preferential nucleation sites to distribute new drops on a condensing surface is explored in this section. The difference in the distribution functions can be seen in Figure 6a. The random and preferential nucleation site approaches represent extremes which are expected to bracket realistic condensation behavior. For low contact angles, the distribution is consistently lower when the drops are distributed at preferential nucleation sites, as opposed to random sites. When the contact angle is low, drops have a large base area; drops that coalesce and remain on the surface cover the "preferential" nucleation sites, and the average drop density is much lower than N_s (average drop density of 3×10^{10} drops/m^2 for the case shown in Figure 6a). When the distribution is random, the number of new drops is governed by the exposed area not covered by drops, and the average drop density on the surface is much higher than in the preferential case, though still lower than N_s (average drop density of 9.5×10^{10} drops/m^2 for the case shown in Figure 6a). In contrast, when the contact angle is high, the distribution for preferential nucleation sites is higher for smaller drops but lower for larger drops. The base area is smaller at higher contact angles, and when small drops coalesce, the resulting composite drop shifts just enough that the base no longer covers the "preferential" site, as described by Rykaczewski et al.[58] This results in an average drop density slightly higher than N_s (1.07×10^{11} drops/m^2), in contrast to the random approach where the average drop density can never exceed N_s. The approach for distributing new nucleation sites influences the drop-size distribution and average nucleation density.

Though the distribution functions are instructive, the time averaged heat transfer rate is the most relevant outcome when considering the influence of the various approaches for distributing drops. As shown in Figure 6b, the random nucleation scheme consistently results in approximately 25% higher rates of heat transfer, regardless of the contact angle or maximum radius size. Notably, even in the case of large contact angles where the distribution function for preferential nucleation is much larger for smaller radii, the total heat transfer rate is still lower since the heat transfer rate for smaller drops is so much smaller. It is supposed that realistic condensation behavior would fall somewhere between these two new drop nucleation extremes, depending on the properties of the condensing surface. Thus, the two approaches may be used to bracket the expected condensation behavior.

Influence of the Nucleation Site Density. On any condensing surface, nucleation site density is governed by the physiochemical properties of the substrate, surface subcooling, atmospheric pressure, and surface texturing.[37,47,63] Since the nucleation site density is difficult to predict as a function of these properties/conditions, nucleation site density is a user-defined input condition to the simulation. This section discusses how changing the nucleation site density changes the drop-size distribution. For drops in the direct-condensation-dominated growth regime, nucleation site density, N_s, influences the distribution, as shown in Figure 7. The variation

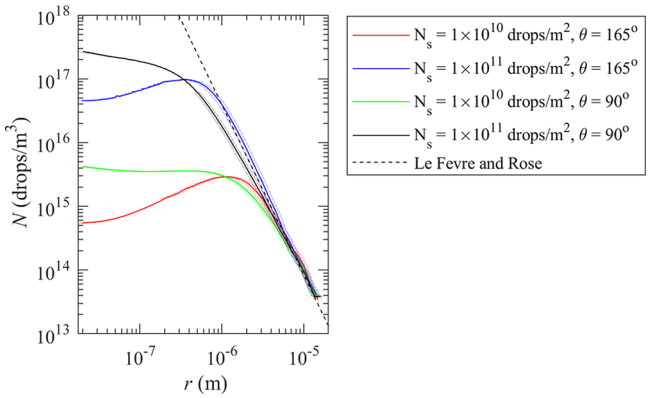

Figure 7. Influence of initial nucleation site density on the distribution function. The distributions shown were produced using the Adhikari heat transfer model, the random nucleation scheme, and $r_{max} = 2 \times 10^{-5}$ m. Drop-size distribution for small drops is highly dependent on the nucleation site density, as predicted by Kim and Kim.[12] Though only distribution functions produced with the random nucleation scheme are shown in the figure, the effect of nucleation site density is the same for the preferential nucleation scheme.

with nucleation site density generally follows the trend predicted by Kim and Kim,[12] where the shape for different nucleation densities is generally similar to deviation observed where the distribution converges with the Le Fevre and Rose correlation.[11] As expected, the time-averaged heat transfer rate is reduced when the nucleation site density is smaller since there are fewer drops condensing. Reducing the nucleation site density from 1×10^{11} drops/m^2 to 1×10^{10} drops/m^2 reduces the overall heat transfer rate by approximately 60% for a 165° contact angle and 40% for a 90° contact angle, assuming conditions consistent with Figure 7 (Adhikari heat transfer model, the random nucleation scheme, and $r_{max} = 2 \times 10^{-5}$ m).

As predicted by previous investigators[12,13,25,37] and shown with the present simulation, initial nucleation site density N_s significantly influences the size at which drops begin to coalesce and size at which the distribution function approaches the empirical Le Fevre and Rose[11,19] correlation. Nucleation site density can be difficult to measure and to predict, though it is influenced by the physiochemical properties of the substrate, surface subcooling, and atmospheric pressure, as well as surface texturing.[37,47,63] While it would be desirable to be able to predict the heat transfer rate as a function of surface subcooling, the ability to predict $N_s(\Delta T)$ is a prerequisite.

The influence of varying the contact angle on the distribution function is also evident in Figure 7. For a contact angle of 165° the distribution generally slightly overshoots the

DOI: 10.1021/acs.langmuir.9b02232
Langmuir 2019, 35, 12858−12875

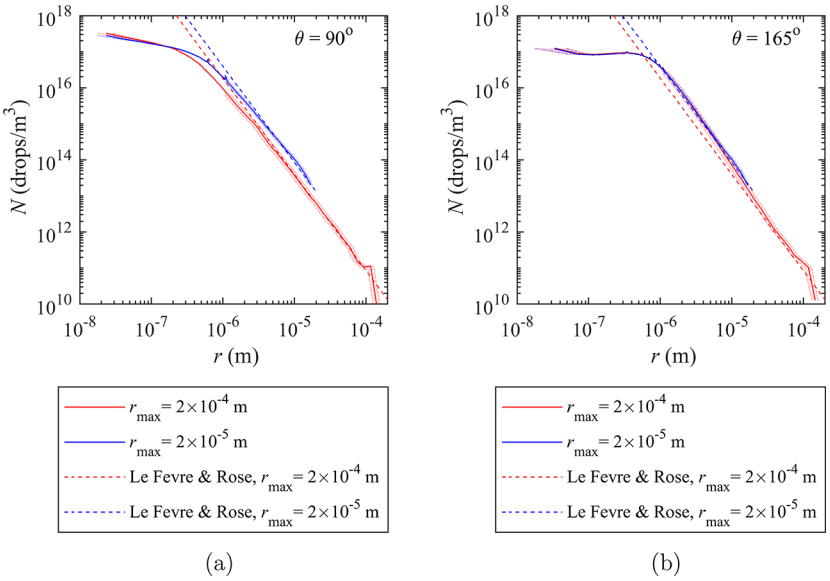

Figure 8. Distribution functions created using the Adhikari model with a contact angle of (a) 90° and (b) 165°. When the contact angle is large, the distribution function is similar for large and small r_{max}.

power law correlation. When the contact angle is 90°, the distribution generally undershoots the power law correlation.

Influence of Maximum Drop Size and Contact Angle. The influence of maximum drop size and contact angle on the drop-size distribution and overall heat transfer rate are explored in this section. Maximum drop size and contact angle are physical properties related to the condensing surface and can easily be determined experimentally for a given surface. Though the maximum drop size is related to the contact angle hysteresis, they are varied independently here to separate their influence, but it should be noted that surfaces with small contact angles (relative to the range tested here) and small maximum drop sizes are unrealistic. The influence of r_{max} on the Le Fevre and Rose correlation[11,19] is generally to shift the drop distribution to the left or the right. When the contact angle is 90°, the simulation predicts that increasing r_{max} will shift the distribution function to the left, as shown in Figure 8. However, when the contact angle is 165°, increasing r_{max} does not shift the distribution function, and the distribution with large r_{max} resembles that of small r_{max} until it diverges to the corresponding power law curve. The cause for this can be understood by recognizing that as the contact angle increases, the area of the base decreases. In the extreme case where the contact angle approaches 180° and the base area approaches zero, it is clear that the maximum size of the drops would have much less influence on the distribution of smaller drops, which would easily fit in the shadow of the larger drops. In the case where drops have contact angles of 165°, the area of the base is still small, covering 5 and 10% of the total area for $r_{max} = 2 \times 10^{-5}$ and 2×10^{-4} m, respectively. Though the area of the substrate covered is twice as high for $r_{max} = 2 \times 10^{-4}$ m, the number of new drops only changes by 5% since the number of new drops is governed by eq 6.

The influence of r_{max} on heat transfer rate can be seen in Figure 9. When the contact angle is 90°, the heat transfer rate generally follows the trend predicted by the Kim and Kim[12] and Miljkovic et al.[13] models, with slight offsets for the difference in heat transfer model and nucleation scheme. However, when the contact angle is 165°, the simulation predicts that the heat transfer rate changes negligibly with r_{max},

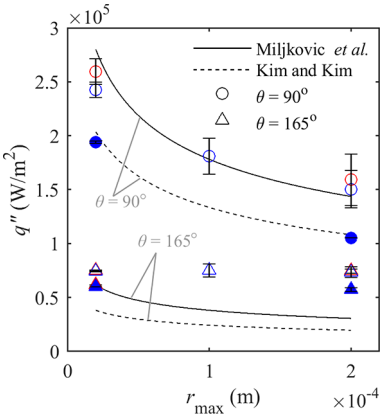

Figure 9. Time-averaged heat transfer rate predicted by the simulation compared with previous models as a function of the contact angle, θ. Results based on the Chavan heat transfer model are shown in red, while the results based on the Adhikari model are shown in blue. Filled markers indicate selection of the preferential nucleation approach to distribute nucleation sites; empty markers indicate the random nucleation approach. The simulation predicts that the heat transfer rates remains constant with increasing maximum drop size at high contact angles.

in contrast to the trend predicted by previous models. In the simulation, the heat transfer rate changes little with r_{max} due to the extremely small base area when the contact angle is high, as discussed in the previous paragraph. The predicted heat transfer rate is extremely sensitive (changing on the order of 50%) to the maximum drop size when the contact angle is low, but relatively insensitive (changing less than the uncertainty) when the contact angle is high. The simulation for $\theta = 165°$ predicts a heat transfer rate on the order of two times higher than the models when $r_{max} = 2 \times 10^{-4}$ m. At high contact angles it may be particularly hazardous to use previously proposed distribution models.

It should be noted that r_{max} is dependent on both the advancing contact angle and contact angle hysteresis. In order to simplify the parameter space and produce results independent of surface type, they have been considered

DOI: 10.1021/acs.langmuir.9b02232
Langmuir 2019, 35, 12858−12875

independently in the present work. However, a surface with θ = 90° and r_{max} = 2 × 10^{-5} m is not physically realistic since surfaces with θ = 90° tend to have large contact angle hysteresis and maximum drop sizes on the order of 1−2 mm. Therefore, while it may appear as though a smaller contact angle would produce higher rates of heat transfer, this is only true as long as the maximum drop sizes were the same. Generally surfaces with higher drop mobility and smaller maximum drop sizes have larger contact angles.

The influence of contact angle on heat transfer rate is indicated in Figure 10 (see also Figure 5). When the contact angle is 90°, the simulation predicts results similar to those of Miljkovic et al.,[13] but as the contact angle increases the heat transfer rate converges regardless of the maximum drop size or heat transfer model. This has important implications for design of superhydrophobic condensing surfaces. Conventional wisdom supposed that the rate of condensation heat transfer is inversely proportional to the diameter of the condensate drops,[10,37,63,65,66] which is true when the contact angle is low. However, at high contact angles the area of the base is so small that the presence of large drops does not significantly influence the surface area available for condensation, and the heat transfer rate is similar regardless of the maximum drop size, assuming the drops are still in a mobile, suspended, or partially wetting state.

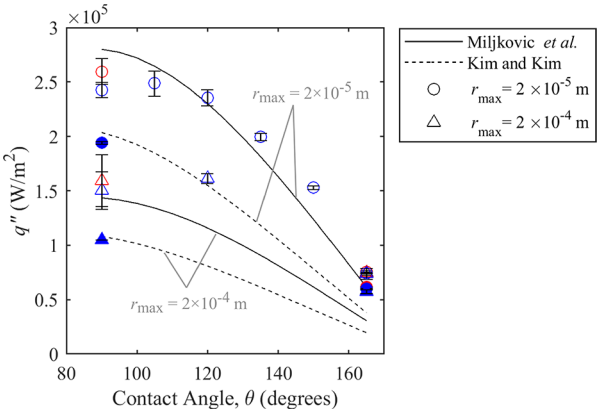

Figure 10. Time-averaged heat transfer rate predicted by the simulation compared with previous models as a function of the maximum drop size on the surface, r_{max}. Results based on the Chavan heat transfer model are shown in red, while the results based on the Adhikari model are shown in blue. Filled markers indicate selection of the preferential nucleation approach to distribute nucleation sites; empty markers indicate the random nucleation approach. The simulation predicts that the heat transfer rates converge to a single rate at large contact angles.

Coalescence-Induced Jumping. The influence of droplet departure via coalescence-induced jumping on the distribution function and heat transfer rate is now considered. Since superhydrophobic surfaces with low adhesion are necessary for coalescence-induced jumping, all simulations which include jumping have a specified contact angle of 165°. The distribution functions for several simulations involving jumping are shown in Figure 11a. For jumping to occur, at least two of the drops involved in the coalescence event must be larger than the minimum jumping radius, r_j. As r_j increases, the maximum size of drops on the surface increases since fewer coalescence events result in jumping and departure, and more drops are allowed to grow larger prior to departure. For small drop radii where drops experience direct-condensation-dominated growth, larger r_j shifts the distribution up slightly since fewer drops are departing from the surface. At r_j = 1 × 10^{-5} m the distribution function becomes very similar to that for which no jumping occurs.

The heat transfer rate increases with increasing r_j until convergence with the no jumping case, as shown in Figure 11b. When r_j is sufficiently small, the simulation predicts higher rates of heat transfer when using the preferential nucleation scheme (as opposed to the random nucleation scheme) since the distribution with preferential nucleation is higher for r < 8 × 10^{-7} m (see Figure 6a and accompanying discussion). The Miljkovic et al.[13] model for jumping is also shown in Figure 11b. In their model, all coalescence and departure occurs at $r = r_e = 1/(4\sqrt{N_s})$ (which corresponds to r_e = 8 × 10^{-7} m when N_s = 1 × 10^{11} drops/m^2), which eliminates the heat transfer that would be contributed by drops larger than this size. The immediate termination of the distribution curve at

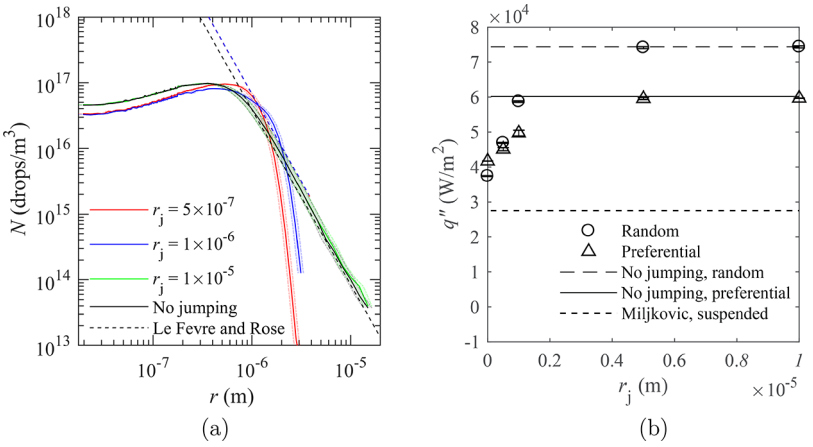

Figure 11. (a) Distribution function when drops larger than r_j depart via coalescence-induced jumping. (b) Heat transfer as a function of r_j. When r_j is sufficiently small, the simulation predicts higher heat transfer rates with the preferential than random nucleation scheme since the distribution is higher for drops in this size range (see Figure 6 and the accompanying discussion). In this example case, the simulation predicts the heat transfer rate decreases with decreasing drop departure size, illustrating the need for drop-size distribution models which account for coalescence at various sizes.

DOI: 10.1021/acs.langmuir.9b02232
Langmuir 2019, 35, 12858−12875

$r = 1/(4\sqrt{N_s})$ explains the significantly lower predicted rate of heat transfer.

Interestingly, in this example case ($N_s = 1 \times 10^{11}$ drops/m^2), prohibiting jumping at smaller sizes (increasing r_j) increases the overall heat transfer rate since drops larger than 5×10^{-7} m comprise a significant portion of the total heat transfer rate when they do not depart, as illustrated in Figure 12. In this figure, the product of the $N(r)$ and $q_d(r)$, the integral of which is q'', is shown as a function of r. When $r_j = 5 \times 10^{-7}$ m, the rate of heat transfer for drops smaller than 2×10^{-6} m is much higher than for $r_j = 1 \times 10^{-5}$ m, but the total heat transfer rate (for $r_j = 1 \times 10^{-5}$ m) is still higher (than for $r_j = 5 \times 10^{-7}$ m) since drops larger than 2×10^{-6} m contribute significantly to the overall heat transfer rate. If drops are too small when they depart, the heat transfer rate is diminished, since they could have contributed significantly to the overall heat transfer rate had they remained on the surface longer. As discussed above, when the contact angle is high, the presence of larger drops does not negatively influence the overall heat transfer rate due to the small base area, as illustrated by Figure 9. However, these results suggest that removing drops that are too small can actually decrease the overall rate of heat of heat transfer, indicating that minimizing drop departure size may not always maximize heat transfer rate. This is contrary to that for surfaces without coalescence-induced jumping.[10] It should be noted that, for surfaces without coalescence-induced jumping, the departure size is the maximum drop size, whereas in the case of coalescence-induced jumping a departure range exists, from the minimum (in this case, r_j) to the maximum. In this case, reducing r_j reduces both the minimum and maximum size of drops on the surface; however, the important parameter for predicting overall heat transfer is neither the maximum nor minimum departure size, but total drop-size distribution, which results from the drop departure size range.

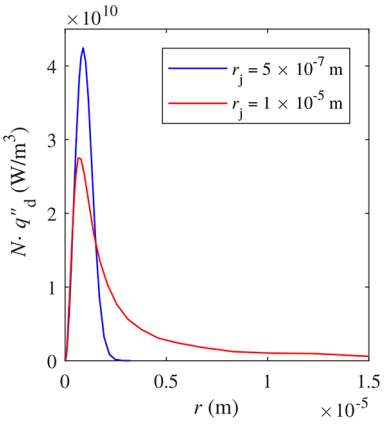

Figure 12. Product of the distribution function and heat transfer rate to a single drop, the integral of which is the overall heat transfer rate, q″. The contribution of larger drops is significant and allowing them to depart at smaller sizes decreases the overall heat transfer rate. The contact angle in the case shown is $\theta = 165°$.

In the present work, coalescence resulting in drop departure is determined based on a specified minimum jumping size; however, the structure of the simulation allows for the use of more sophisticated models for drop jumping. For example, a model for jumping based on an energy balance between the adhesive force of the drops and energy released upon coalescence could be evaluated for each coalescence event, enabling the inclusion of factors such as surface feature length scale, drop wetting state, relative size mismatch, and number of drops involved in a coalescence event, all of which have been shown to influence drop departure.[32−34,40,53,59,67,68] Inclusion of additional drop departure criteria in the simulation may alter the drop-departure-size distribution, drop-size distribution, and overall heat transfer rate.

The results from the simulation suggest that removing large drops (by changing the minimum drop departure size) may not always lead to increased overall heat transfer rates since large drops do not cover a significant portion of the surface when the contact angle is large. In addition, drops similar in size to those departing by coalescence-induced jumping can still contribute significantly to the overall heat transfer rate. The point that minimizing drop size does not always maximize heat transfer appears to contradict the prevalent idea that heat transfer rate is inversely proportional to the diameter of the condensate drops; however, this has only been shown to be true for lower contact angle surfaces without removal by coalescence-induced jumping.[10,37,63,65,66] The results from the present simulation show that the heat transfer rate is not inversely proportional to drop size when coalescence-induced jumping occurs, since smaller drops still contribute significantly to heat transfer.

Besides the reasons discussed in the present work, others have shown additional reasons that minimizing drop size does not always increase heat transfer. Birbarah and Miljkovic showed that minimizing drop departure size is not always beneficial for heat transfer since smaller departed drops may return to the surface due to the vapor flux.[69] An individual drop heat transfer model from Xu et al. suggests that larger drops may have higher heat transfer rates than originally anticipated when internal drop convection is considered, which means that larger drops would be even larger contributors to the overall heat transfer rate than predicted with the current individual drop heat transfer models.[64] Mendoza et al. demonstrated that noncontinuum and interface curvature becomes increasingly important with decreasing drop-size. They suggest the achievable heat transfer rate reaches a peak beyond which decreasing the mean drop size will decrease heat transfer. The results from the present simulation, Birbarah and Miljkovic, Xu et al., and Mendoza et al. suggest four completely different reasons that minimizing drop size does not always lead to increased heat transfer rates. An ideal size for drop departure may exist which is significantly larger than the minimum drop-departure size achievable, in contrast to that which has been shown to be true for hydrophobic surfaces without coalescence-induced jumping.

■ CONCLUSION

A computer simulation of dropwise and jumping drop condensation on vertical surfaces was described. Parameters dependent on surface structure and chemistry, including contact angle (θ), maximum drop size (r_{max}), and minimum jumping radius (r_j), are specified to the simulation, so that each parameter may be independently determined for a given surface. The simulation was used to explore the influence of the assumptions of coalescence and jumping at a single drop size, which are used in population balance-based models. The influence of various input parameters corresponding to model assumptions (individual drop heat transfer model and nucleation site distribution approach) and various physical conditions (nucleation site density, maximum drop size,

DOI: 10.1021/acs.langmuir.9b02232
Langmuir 2019, 35, 12858−12875

contact angle, and minimum jumping size) on the drop-size distribution and overall heat transfer rate were also explored. Though other computational models have previously been employed, the contributions of this work offer (1) a computational approach to explore the influence of assumptions in population balance modeling, (2) an exploration of drop-size distributions over a wide range of physical conditions, and (3) an understanding of the impact of various input conditions on the overall heat transfer rate.

Results of the simulation are valid for smooth hydrophobic or nanostructured superhydrophobic surfaces, where the assumptions of constant contact angle growth and negligible thermal resistance at the drop/surface interface are reasonable. The simulation assumes a constant contact angle during drop growth, though this assumption is not expected to significantly influence the results since the simulation is only valid on smooth hydrophobic or nanostructured surfaces. Instantaneous sweeping and coalescence are assumed, as discussed in the text. The simulation also assumes drops are in a suspended or partially wetting, mobile (subject to sweeping) state with spherical-cap shaped drops. Furthermore, the simulation results are limited by the accuracy of the individual drop growth models used, each of which also contains certain assumptions, including growth in the absence of non-condensable gases.

Results of the simulation suggest that population balance methods account for general trends in the drop-size distribution (overall shape and influence of nucleation density) but include certain assumptions (coalescence and departure at a single drop size) that limit their accuracy. In particular, results of the current simulation suggest that setting the transition from direct-condensation-dominated growth to coalescence-dominated growth at $r_e = 1/(4\sqrt{N_s})$ may overestimate the drop-size distribution. With the lack of available experimental data for distributions in this size range, the present work represents the first attempt to evaluate the accuracy of the population balance modeling approach using a numerical simulation.

Both the individual drop heat transfer model and the approach for distributing nucleation sites used in the simulation influences both the distribution and the overall heat transfer rate. The influence of the heat transfer model is particularly significant at low contact angles. For the parameter range explored in the present simulation, the random nucleation scheme resulted in heat transfer rates on the order of 25% larger than those predicted with the preferential nucleation scheme. Realistic nucleation behavior is likely a combination of the two nucleation approaches, and thus the two approaches may be used together to bracket realistic behavior. The individual drop heat transfer model and nucleation site distribution approach affect the final results and should be carefully considered in any condensation model.

A primary contribution of this work is a discussion of the relationship between maximum drop size and heat transfer rate. When the contact angle is large and no jumping occurs, increasing the maximum drop size has a less significant influence on the distribution and overall heat transfer rate since the base area is small. Previous models deviate most from the current results at large contact angles, suggesting that previous models may be less accurate when the contact angle is large. Furthermore, when coalescence-induced jumping occurs, results of the simulation suggest that removing drops at extremely small sizes via coalescence-induced jumping can lead to lower heat transfer rates due to the fact that the heat transfer rate to drops that are removed contributes significantly to the overall heat transfer rate (drops larger than 0.5 μm contribute 25−40% of the total heat transfer for the case in Figure 11). In the cases simulated, the model proposed by Miljkovic et al.[13] under-predicts (on the order of a factor of 2 for the case in Figure 11) the heat transfer rate for jumping drops since it assumes all drops coalesce and depart at a single size. Additionally, the recent work of Xu et al.[64] suggests that convection is a significant contributor to the heat transfer rate for larger drops (becoming significant for drops between 5 and 200 μm, depending on the rate of subcooling and contact angle). Since the models included in this analysis consider only conduction, the heat transfer rate for large drops where convection becomes significant may be under predicted. When convection is included in the model for heat transfer to an individual drop, it may be even more advantageous for large drops to remain on the surface. However, even when not considering convection, the present work suggests that, when the contact angle is large and coalescence-induced jumping occurs, previous models fail to accurately predict the relationship between maximum drop size and heat transfer rate.

METHODS

The present work offers insight into factors which are important when modeling condensation heat transfer. The large parameter space precludes formulation of a closed-form function for the drop-size distribution. The following methods outline the approach to modeling dropwise condensation in this work, and may be adapted with improved approaches as they are developed. The MATLAB code used to perform these simulations will be provided upon request.

Drop Coalescence. The size and location of each drop is used to determine when drops on the surface touch in three-dimensional space. When the shortest distance (d) between a primary drop (p) and a neighboring drop (i) is less than zero, it is concluded that drops are touching according to the following relation,

$$d = \sqrt{(x_p - x_i)^2 + (y_p - y_i)^2 + (r_p - r_i)^2(\cos\theta)^2} - r_p - r_i \tag{8}$$

and as illustrated in Figure 13, where x, y, and r are the x and y locations and radii of each drop. It is possible for more than two drops

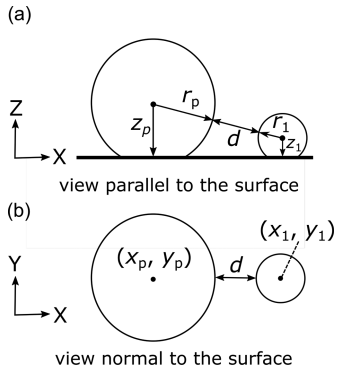

Figure 13. A schematic illustrating the criteria for coalescence. When the distance d between the primary drop p and a neighboring drop (labeled 1) is less than zero, drops will coalesce and the two coalescing parent drops are replaced by a child drop at the center of mass of the parents. The distance from the base to the center of each drop, z, is $r\cos(\theta)$.

DOI: 10.1021/acs.langmuir.9b02232
Langmuir 2019, 35, 12858−12875

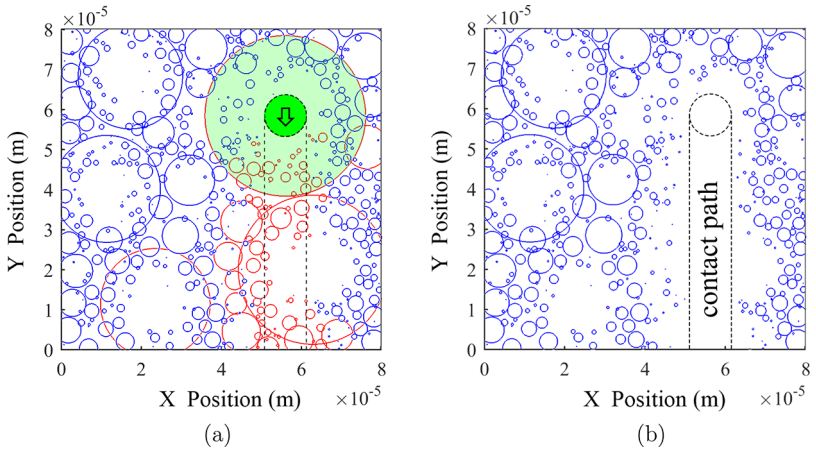

Figure 14. (a) Visualization of the drops in the simulation immediately prior to a sweeping event. Red and blue circles represent the projected area of all drops on the surface. As the large drop (shaded in light green) sweeps downward, it removes all the red drops with which it interacts in its path. The darker green circle indicates the base of the large sweeping drop. The area covered by the base of the sweeping droplet as it sweeps is demarcated with black dashed lines. (b) Visualization of the drops in the simulation immediately following a sweeping event. The portion of the surface in contact with the base of the sweeping drop is outlined with a black dashed line.

to be overlapping at a given time. When checking for overlapping drops, the simulation iterates through each drop (primary drop) and determines which neighboring drops overlap with each primary drop. All neighboring secondary drops are included in the coalescence event and behave as specified by the selected approach for the resulting drop (remain/depart). It is also possible for secondary drops to be overlapping with other drops (tertiary drops). In this case, referred to as chain coalescence, all of the tertiary drops are also included in the coalescence event. Though it is possible for additional drops to be touching the tertiary drops, they are not included in the coalescence event since it is assumed that, when the time step is sufficiently small, their inclusion would have negligible impact on the distribution function and time-averaged heat transfer rate. It is also possible for a coalescence event to result in the creation of a new drop that is large enough to overlap with other drops, referred to as cascading coalescence. However, this possibility is not addressed until the next time step since waiting will not have a significant influence if the time step is sufficiently small. It is possible for both cascading and chain coalescence to occur within the same time step. However, as long as the time step is sufficiently small, the effect of waiting until the next time step to address the cascading part of the coalescence event is again assumed to be negligible.

The assumption that coalescing drops will result in a drop at the center of mass of the parent drops has been validated experimentally,[59,70] and this approach has been used by Mei et al.,[38] Barati et al.[39] and Khandekar and Muralidhar.[47] It includes the assumption that the coalescing drops have a similar morphology and adhesive force. For example, the center of mass assumption may not be true if one drop were highly pinned or in a wetted (Wenzel) state and the other drop in a nonwetting (Cassie) state.

In reality, drop coalescence spans a finite amount of time and, following coalescence, the resulting drop continues to oscillate, potentially interacting with surrounding drops and inducing additional mixing. Postcoalescence mixing delays recovery of the quasi-steady internal temperature profile that is assumed in all of the individual drop heat transfer models employed in this work. Adhikari and Rattner predicted that the assumption of instantaneous coalescence underpredicts total heat transfer by 15−20% in the time immediately following a coalescence event.[71] Incorporation of a correlation accounting for the instantaneous coalescence assumption may improve the accuracy of the simulation work and is identified as potential future work.

Drop Sweeping. When a drop grows to the user-specified maximum radius, r_{max}, gravity-induced sweeping is simulated by removing all of the drops located below it. For simplicity, the initial sweeping drop remains the same size throughout the sweeping event. However, in reality, as a drop travels downward from its center of mass, the sweeping behavior would increase the initial drop size as it coalesces with drops in its path. The influence of assuming a constant drop size during sweeping is expected to be negligibly small when the height of the domain is on the same order as the size of the sweeping drop, as is the case in the present work. An example of a sweeping event for drops with a contact angle of 165° is illustrated in Figure 14, with the light green shading indicating the sweeping drop and the darker green circle indicating the location of the base area in contact with the condensing surface. Red and blue circles represent the projected area of all drops on the surface. The red circles indicate drops that interact and coalesce with a sweeping drop as it moves along the surface. The contact path of the base area during the sweeping motion is demarcated with black dashed lines; clearly, all drops with bases overlapping the area traveled by the sweeping drop will be swept away. Additionally, drops located outside of the path may also interact with a sweeping drop, depending on size and location, as governed by the following equation for the minimum distance, d_s, between the sweeping drop, s, and another drop, i.

$$d_s = \sqrt{(x_s - x_i)^2 + (r_s - r_i)^2(\cos\theta)^2} - r_s - r_i \quad (9)$$

When the minimum distance below the half-height of the sweeping drop is negative, neighboring drops along the sweeping path will interact with the initial sweeping drop as it falls and also be removed. The only difference between eqs 8 and 9 is that the distance in the y direction is omitted, since the sweeping drop moves in that direction. In reality, the length of time required for a drop to sweep the surface is likely longer than a single time step. However, the assumption of instantaneous sweeping is not expected to significantly influence the time-averaged results since the swept area is small relative to the total domain area when averaged over the duration of the entire simulation.

Obtaining the Drop-Size Distribution. The purpose of the simulation is to obtain the steady state distribution for the size of the drops on a surface during condensation, $N(r)$, or the number of drops per unit area as a function of radius size. The time-averaged drop-size distribution is calculated in following manner. A histogram of drop sizes is generated from all of the drops in the simulation and averaged over many specific instances in time so that a minimum of 1×10^7 drops is used to construct each histogram. The histogram bin width is determined in a piece-wise manner. The bin width for smaller drops is defined by the amount that a drop grows in a single time step. For larger drops where the drop size changes by less than 1% in a single time step, the bin width is specified as 25 logarithmically spaced bins. The count is then normalized by the domain size, and the distribution is obtained by dividing the histogram by the bin width, so that the

DOI: 10.1021/acs.langmuir.9b02232
Langmuir 2019, 35, 12858−12875

distribution function has units of drops/m^2/m, or drops/m^3, as described in the following equation.

$$N(r) = \frac{\sum_{s=1}^{S}\sum_{i=1}^{n}\left[r - \frac{1}{2}\Delta r < r_{i,s} < r + \frac{1}{2}\Delta r\right]}{A_d \Delta r S} \quad (10)$$

In this equation, S is the total number of time steps, s is the count through the time step, n is the total number of drops in at a particular time step, r is the radius, A_d is the total domain area, Δr is the bin width, and the brackets denote the Iverson bracket, where the number is 1 if the statement is true and 0 if the statement is false (similar to the Kronecker delta function). The distribution function is always shown with error bounds associated with bin width using light shading, and is often approximately the size of the line (e.g., Figure 5).

Overall Heat Transfer Rate. As the simulation progresses in time, individual drops continue to grow in size. Coalescence and sweeping events occur as outlined above with new drops distributed at each time step. At each time step, the total instantaneous heat transfer rate, q_{inst}'', is the sum of the heat transfer from each individual drop,

$$q_{inst}'' = \frac{\sum_{i=1}^{n} q_{d,i}}{A} \quad (11)$$

where n is the total number of drops in the simulation at each time step. Averaging q_{inst}'' over the entire simulation results in an expression for overall heat transfer rate equivalent to that expressed in eq 1. Estimates of the overall heat transfer rate calculated by multiplying the drop-size distribution from simulation by the individual drop heat transfer rate (eq 1) agreed with that obtained by time averaging eq 11 within the uncertainty associated with time step size.

Steady State Condition. Each simulation is run at least until the condensation has reached a quasi-steady state. As shown in Figure 15,

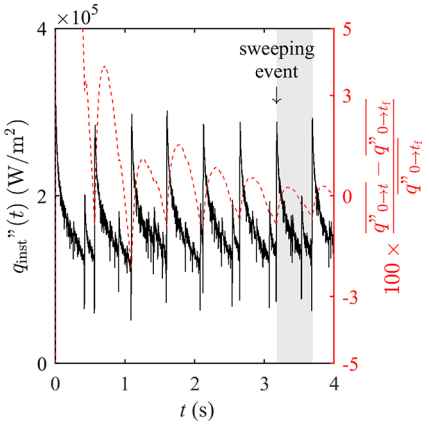

Figure 15. Instantaneous heat transfer rate for a simulation with a contact angle of 90° and r_{max} = 1 × 10^{-4} m. Large spikes occur immediately following a sweeping event. The area shaded in gray indicates the last complete sweeping cycle. The simulation is considered to have reached steady state when the time-averaged heat transfer rate (as shown on the right ordinate) changes by less than 5% over the course of the last sweeping cycle (typically <1%).

the instantaneous heat transfer rate spikes following the departure of a drop, where the last complete sweeping cycle is highlighted in gray. Quasi-steady state is defined as the point where the time-averaged heat transfer rate (averaged from the start of the simulation to time t), $\overline{q''}_{0\to t}$, changes <5% relative to the final time-averaged heat transfer rate, $\overline{q''}_{0\to t_f}$, during the last sweeping cycle, as described in eq 12 and shown in Figure 15.

$$\text{percent change} = 100 \times \frac{\overline{q''}_{0\to t} - \overline{q''}_{0\to t_f}}{\overline{q''}_{0\to t_f}} \quad (12)$$

For the case shown, the requirement of <5% change is met after the first complete sweeping cycle, around 1 s. Typically, simulations are run much longer than that required by <5% change over the course of the last sweeping cycle resulting in many sweeping cycles and <1% change in the time-averaged heat transfer rate. When θ is low and R_{max} is large, the instantaneous heat transfer rate changes more dramatically with each sweeping event. However, large R_{max} requires large domain sizes, and require long computational time; therefore, large simulations were run for the minimum amount of time required to meet the requirement for <5% change over the course of the last sweeping cycle.

Time Grid Independence. Selection of the time step has important implications for the accuracy of the simulation, where smaller time steps produce more accurate results at the cost of increased computation time. Time step size influences simulation accuracy with the assumptions of linear individual drop growth rate (see eq 4), instantaneous sweeping, coalescence, and jumping, as well as the importance of the relative order of the events in Figure 1, which are treated sequentially during the course of a single time step. In the limit of an infinitely small time step, the influence of linear drop growth rate, instantaneous coalescence and the sequence of drop events during a single time step is negligible. Therefore, each simulation was run at multiple time steps to establish time grid independence. The distribution function $N(r)$ is shown in Figure 16

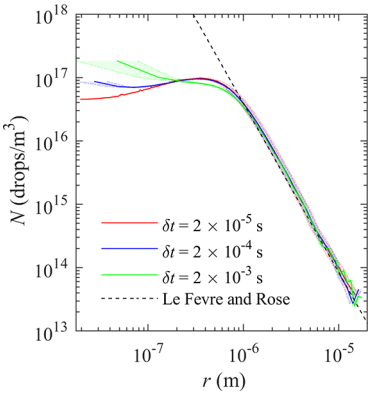

Figure 16. Distribution functions obtained from simulations run with time steps of varying size. In large drop range, the distribution functions converge, indicating that the simulation is time grid independent for that size. Distribution functions diverge with decreasing radii, where the distribution function is no longer time grid independent.

for simulations run with decreasing time step. The distribution functions converge at larger radii and diverge at smaller radii, as shown for the selected time steps. The distribution is considered grid independent until divergence in the distribution functions with decreasing radius. In order to establish the time-averaged heat flux, q'', at least three simulations of decreasing time step were run for each condition tested, and the grid-convergence index was calculated following the method described by Roache,[72] using generalized Richardson extrapolation, thus quantifying the uncertainty associated with time step size. Uncertainty limits are reported with error bars for each time-averaged heat flux, though in some cases the error bars are too small to distinguish in the figures.

Domain Size Selection. The simulation consists of a square domain with side length L. The number of drops in the simulation and the corresponding computational time increases with the square of the domain area. Therefore, it is desirable to limit the domain size as much as possible without sacrificing accuracy. The domain size was chosen so that $2r_{max}/L$ < 0.8, ensuring that the largest drop never

DOI: 10.1021/acs.langmuir.9b02232
Langmuir 2019, 35, 12858−12875

covered the entire domain. Satisfying this criteria produced both distribution functions and time-averaged heat transfer rates that were largely independent of domain size (no discernible difference in distribution function and difference in heat transfer rates smaller than the time-grid convergence uncertainty), though smaller domain sizes (relative to the maximum drop size) were not tested and may also produce domain-size independent results.

Constant Contact Angle. Drop growth with constant contact angle is assumed in the simulation. Although it is well-known that the contact angle changes as drops grow,[13,29,30,56,58,73−75] for a smooth hydrophobic or nanostructured superhydrophobic surface the size range where drops are growing with a nonconstant contact angle is relatively small in comparison to the total drop-size range.[13,29,75] At any given time, drops that would be growing with a nonconstant contact angle account for a small fraction of the total area covered on the surface and therefore contribute only a small amount toward the total heat transfer. In order to ensure that using a constant contact angle would not significantly influence the accuracy of the results, simulations were conducted where the contact angle varied as proposed by Miljkovic et al.[13] for a partially wetting drop on a surface with features of length scale 100 nm, intrinsic contact angle $\theta_a = 90°$, apparent contact angle when in the Cassie−Baxter state $\theta_a^{CB} = 165°$, and $r_{max} = 2 \times 10^{-5}$ m. Selecting a small r_{max} results in a contact angle change over a larger percentage of the range of drops on the surface, making this test scenario an extreme example. The Chavan heat transfer model is used since the Adhikari model requires a separate curve fit for each contact angle. Nucleation sites were selected randomly, drops did not experience jumping, and the initial nucleation site density was $N_s = 1 \times 10^{11}$ drops/m^2. The radius where the contact angle becomes constant, r_{CCA}, is 3.86×10^{-7} m. In this extreme case, varying the contact angle resulted in <2.6% difference in the time-averaged heat transfer rate. Given that drops smaller than r_{CCA} accounted for <1% of the surface area covered by drops, this is not a surprising result, and strengthens the argument that using a constant contact angle does not significantly influence the accuracy of the results. Furthermore, by maintaining a constant contact angle, the distribution functions obtained from the simulation are applicable for all smooth hydrophobic and nanostructured surfaces and are not tied to specific surface properties. Since r_{max} is specified in the simulation, the receding and static contact angles are never specified, and a single contact angle, θ (which may be thought of as the advancing contact angle) is used throughout the simulation.

Contact angle varies more appreciably on microstructured surfaces where inclusion of a nonconstant contact angle may have a more significant impact on the distribution function and heat transfer rate. The impact of varying contact angle should be explored before using the constant contact angle assumption with microstructured surfaces.[13,29,75]

AUTHOR INFORMATION

Corresponding Author

*E-mail: bdiverson@byu.edu.

ORCID

Brian D. Iverson: 0000-0002-4592-3728

Notes

The authors declare no competing financial interest.

ACKNOWLEDGMENTS

This material is based upon work supported by the National Science Foundation under Grant No. 1805805 and the Utah NASA Space Grant Consortium under Grant No. NNX15A124H.

REFERENCES

(1) Khawaji, A. D.; Kutubkhanah, I. K.; Wie, J.-M. Advances in seawater desalination technologies. *Desalination* **2008**, *221*, 47−69.

(2) Andrews, H. G.; Eccles, E. A.; Schofield, W. C.; Badyal, J. P. Three-dimensional hierarchical structures for fog harvesting. *Langmuir* **2011**, *27*, 3798−3802.

(3) Humplik, T.; Lee, J.; O'Hern, S. C.; Fellman, B. A.; Baig, M. A.; Hassan, S. F.; Atieh, M. A.; Rahman, F.; Laoui, T.; Karnik, R.; Wang, E. N. Nanostructured materials for water desalination. *Nanotechnology* **2011**, *22*, 292001.

(4) Beér, J. M. High efficiency electric power generation: The environmental role. *Prog. Energy Combust. Sci.* **2007**, *33*, 107−134.

(5) Attinger, D.; Frankiewicz, C.; Betz, A. R.; Schutzius, T. M.; Ganguly, R.; Das, A.; Kim, C.-J.; Megaridis, C. M. Surface engineering for phase change heat transfer: A review. *MRS Energy and Sustainability* **2014**, *1*, 1−40.

(6) Lee, A.; Moon, M.-W.; Lim, H.; Kim, W.-D.; Kim, H.-Y. Water harvest via dewing. *Langmuir* **2012**, *28*, 10183−10191.

(7) Vasiliev, L. L. Heat pipes in modern heat exchangers. *Appl. Therm. Eng.* **2005**, *25*, 1−19.

(8) Pérez-Lombard, L.; Ortiz, J.; Pout, C. A review on buildings energy consumption information. *Energy and Buildings* **2008**, *40*, 394−398.

(9) Schmidt, E.; Schurig, W.; Sellschopp, W. Versuche über die Kondensation von Wasserdampf in Film- und Tropfenform. *Forsch. Ingenieurwes.* **1930**, *1*, 53−63.

(10) Rose, J. W. Dropwise condensation theory and experiment: A review. *Proc. Inst. Mech. Eng., Part A* **2002**, *216*, 115−128.

(11) Le Fevre, E. J.; Rose, J. W. A Theory of Heat Transfer by Dropwise Condensation. *Proceedings of the Third International Heat Transfer Conference* **1966**, *2*, 362−375.

(12) Kim, S.; Kim, K. J. Dropwise Condensation Modeling Suitable for Superhydrophobic Surfaces. *J. Heat Transfer* **2011**, *133*, 081502.

(13) Miljkovic, N.; Enright, R.; Wang, E. N. Modeling and optimization of superhydrophobic condensation. *J. Heat Transfer* **2013**, *135*, 111004.

(14) Miljkovic, N.; Enright, R.; Nam, Y.; Lopez, K.; Dou, N.; Sack, J.; Wang, E. N. Jumping-droplet-enhanced condensation on scalable superhydrophobic nanostructured surfaces. *Nano Lett.* **2013**, *13*, 179−187.

(15) Miljkovic, N.; Wang, E. N. Condensation heat transfer on superhydrophobic surfaces. *MRS Bull.* **2013**, *38*, 397−406.

(16) Chen, X.; Wu, J.; Ma, R.; Hua, M.; Koratkar, N.; Yao, S.; Wang, Z. Nanograssed Micropyramidal Architectures for Continuous Dropwise Condensation. *Adv. Funct. Mater.* **2011**, *21*, 4617−4623.

(17) Cho, H. J.; Preston, D. J.; Zhu, Y.; Wang, E. N. Nanoengineered materials for liquid-vapour phase-change heat transfer. *Nature Reviews Materials* **2017**, *2*, 16092.

(18) Enright, R.; Miljkovic, N.; Alvarado, J. L.; Kim, K.; Rose, J. W. Dropwise Condensation on Micro- and Nanostructured Surfaces. *Nanoscale Microscale Thermophys. Eng.* **2014**, *18*, 223−250.

(19) Rose, J. W.; Glicksman, L. R. Dropwise condensation−The distribution of drop sizes. *Int. J. Heat Mass Transfer* **1973**, *16*, 411−425.

(20) Tanasawa, I.; Tachibana, F. A synthesis of the total process of dropwise condensation using the method of computer simulation. *Proceedings of the 4th International Heat Transfer Conference* **1970**, 1−11.

(21) Tanaka, H. A Theoretical Study of Dropwise Condensation. *J. Heat Transfer* **1975**, *97*, 72−78.

(22) Watanabe, N.; Aritomi, M.; Machida, A. Time-series characteristics and geometric structures of drop-size distribution density in dropwise condensation. *Int. J. Heat Mass Transfer* **2014**, *76*, 467−483.

(23) Wen, R.; Lan, Z.; Peng, B.; Xu, W.; Ma, X. Droplet dynamics and heat transfer for dropwise condensation at lower and ultra-lower pressure. *Appl. Therm. Eng.* **2015**, *88*, 265−273.

(24) Wen, H. W.; Jer, R. M. On the heat transfer in dropwise condensation. *Chemical Engineering Journal* **1976**, *12*, 225−231.

(25) Maa, J. R. Drop size distribution and heat flux of dropwise condensation. *Chemical Engineering Journal* **1978**, *16*, 171−176.

(26) Abu-Orabi, M. Modeling of heat transfer in dropwise condensation. *Int. J. Heat Mass Transfer* **1998**, *41*, 81−87.

DOI: 10.1021/acs.langmuir.9b02232
Langmuir 2019, 35, 12858−12875

(27) Law, K.-Y. Definitions for Hydrophilicity, Hydrophobicity, and Superhydrophobicity: Getting the Basics Right. *J. Phys. Chem. Lett.* **2014**, *5*, 686−688.
(28) Chen, W.; Fadeev, A. Y.; Hsieh, M. C.; Oner, D.; Youngblood, J.; McCarthy, T. J. Ultrahydrophobic and ultralyophobic surfaces: Some comments and examples. *Langmuir* **1999**, *15*, 3395−3399.
(29) Enright, R.; Miljkovic, N.; Al-Obeidi, A.; Thompson, C. V.; Wang, E. N. Condensation on Superhydrophobic Surfaces: The Role of Local Energy Barriers and Structure Length Scale. *Langmuir* **2012**, *28*, 14424−14432.
(30) Miljkovic, N.; Enright, R.; Wang, E. N. Effect of droplet morphology on growth dynamics and heat transfer during condensation on superhydrophobic nanostructured surfaces. *ACS Nano* **2012**, *6*, 1776−1785.
(31) Boreyko, J. B.; Chen, C.-H. Self-Propelled Dropwise Condensate on Superhydrophobic Surfaces. *Phys. Rev. Lett.* **2009**, *103*, 184501.
(32) Enright, R.; Miljkovic, N.; Sprittles, J.; Nolan, K.; Mitchell, R.; Wang, E. N. How Coalescing Droplets Jump. *ACS Nano* **2014**, *8*, 10352−10362.
(33) Cha, H.; Xu, C.; Sotelo, J.; Chun, J. M.; Yokoyama, Y.; Enright, R.; Miljkovic, N. Coalescence-induced nanodroplet jumping. *Physical Review Fluids* **2016**, *1*, 064102.
(34) Mouterde, T.; Lehoucq, G.; Xavier, S.; Checco, A.; Black, C. T.; Rahman, A.; Midavaine, T.; Clanet, C.; Quéré, D. Antifogging abilities of model nanotextures. *Nat. Mater.* **2017**, *16*, 658−663.
(35) Zhang, L.; Xu, Z.; Lu, Z.; Du, J.; Wang, E. N. Size distribution theory for jumping-droplet condensation. *Appl. Phys. Lett.* **2019**, *114*, 163701.
(36) Gose, E. E.; Mucciardi, A. N.; Baer, E. Model for dropwise condensation on randomly distributed sites. *Int. J. Heat Mass Transfer* **1967**, *10*, 15−22.
(37) Glicksman, L. R.; Hunt, A. W. Numerical Simulation of Dropwise Condensation. *Int. J. Heat Mass Transfer* **1972**, *15*, 2251−2269.
(38) Mei, M.; Hu, F.; Han, C.; Cheng, Y. Time-averaged droplet size distribution in steady-state dropwise condensation. *Int. J. Heat Mass Transfer* **2015**, *88*, 338−345.
(39) Boroomandi Barati, S.; Pionnier, N.; Pinoli, J. C.; Valette, S.; Gavet, Y. Investigation spatial distribution of droplets and the percentage of surface coverage during dropwise condensation. *Int. J. Therm. Sci.* **2018**, *124*, 356−365.
(40) Meng, K.; Fan, W.; Wang, H. Dynamic scenario simulation of dropwise condensation on a superhydrophobic surface with droplet jumping. *Appl. Therm. Eng.* **2019**, *148*, 316−323.
(41) Birbarah, P.; Chavan, S.; Miljkovic, N. Numerical Simulation of Jumping Droplet Condensation. *Langmuir* **2019**, *35*, 10309−10321.
(42) Leach, R. N.; Stevens, F.; Langford, S. C.; Dickinson, J. T. Dropwise condensation: experiments and simulations of nucleation and growth of water drops in a cooling system. *Langmuir* **2006**, *22*, 8864−8872.
(43) Fritter, D.; Knobler, C. M.; Beysens, D. A. Experiments and simulation of the growth of droplets on a surface (breath figures). *Phys. Rev. A: At., Mol., Opt. Phys.* **1991**, *43*, 2858−2869.
(44) Family, F.; Meakin, P. Scaling of the Droplet-Size Distribution in Vapor-Deposited Thin-Films. *Phys. Rev. Lett.* **1988**, *61*, 428−431.
(45) Meakin, P. Dropwise condensation: the deposition growth and coalescence of fluid droplets. *Phys. Scr.* **1992**, *1992*, 31−41.
(46) Burnside, B. M.; Hadi, H. A. Digital computer simulation of dropwise condensation from equilibrium droplet to detectable size. *Int. J. Heat Mass Transfer* **1999**, *42*, 3137−3146.
(47) Khandekar, S.; Muralidhar, K. Dropwise Condensation on Inclined Textured Surfaces. *Dropwise Condensation on Inclined Textured Surfaces* **2014**, 1−141.
(48) Carey, V. P. *Liquid-vapor phase-change phenomena: An introduction to the thermophysics of vaporization and condensation processes in heat transfer equipment*; Taylor and Francis: New York, 2008.
(49) Chavan, S.; Cha, H.; Orejon, D.; Nawaz, K.; Singla, N.; Yeung, Y. F.; Park, D.; Kang, D. H.; Chang, Y.; Takata, Y.; Miljkovic, N. Heat Transfer through a Condensate Droplet on Hydrophobic and Nanostructured Superhydrophobic Surfaces. *Langmuir* **2016**, *32*, 7774−7787.
(50) Adhikari, S.; Nabil, M.; Rattner, A. S. Condensation heat transfer in a sessile droplet at varying Biot number and contact angle. *Int. J. Heat Mass Transfer* **2017**, *115*, 926−931.
(51) Mulroe, M. D.; Srijanto, B. R.; Ahmadi, S. F.; Collier, C. P.; Boreyko, J. B. Tuning Superhydrophobic Nanostructures To Enhance Jumping-Droplet Condensation. *ACS Nano* **2017**, *11*, 8499−8510.
(52) Li, G.; Alhosani, M. H.; Yuan, S.; Liu, H.; Ghaferi, A. A.; Zhang, T. Microscopic Droplet Formation and Energy Transport Analysis of Condensation on Scalable Superhydrophobic Nanostructured Copper Oxide Surfaces. *Langmuir* **2014**, *30*, 14498−14511.
(53) Kim, M.-K.; Cha, H.; Birbarah, P.; Chavan, S.; Zhong, C.; Xu, Y.; Miljkovic, N. Enhanced Jumping-Droplet Departure. *Langmuir* **2015**, *31*, 13452−13466.
(54) Wen, R.; Xu, S.; Zhao, D.; Lee, Y.-C.; Ma, X.; Yang, R. Hierarchical Superhydrophobic Surfaces with Micropatterned Nanowire Arrays for High-Efficiency Jumping Droplet Condensation. *ACS Appl. Mater. Interfaces* **2017**, *9*, 44911−44921.
(55) Wen, R.; Xu, S.; Ma, X.; Lee, Y.-C.; Yang, R. Three-Dimensional Superhydrophobic Nanowire Networks for Enhancing Condensation Heat Transfer. *Joule* **2018**, *2*, 269−279.
(56) Enright, R.; Miljkovic, N.; Dou, N.; Nam, Y.; Wang, E. N. Condensation on Superhydrophobic Copper Oxide Nanostructures. *J. Heat Transfer* **2013**, *135*, 091304.
(57) Cao, P.; Xu, K.; Varghese, J. O.; Heath, J. R. The Microscopic Structure of Adsorbed Water on Hydrophobic Surfaces under Ambient Conditions. *Nano Lett.* **2011**, *11*, 5581−5586.
(58) Rykaczewski, K.; Scott, J. H. J.; Rajauria, S.; Chinn, J.; Chinn, A. M.; Jones, W. Three dimensional aspects of droplet coalescence during dropwise condensation on superhydrophobic surfaces. *Soft Matter* **2011**, *7*, 8749−8752.
(59) Cha, H.; Chun, J. M.; Sotelo, J.; Miljkovic, N. Focal Plane Shift Imaging for the Analysis of Dynamic Wetting Processes. *ACS Nano* **2016**, *10*, 8223−8232.
(60) Rykaczewski, K.; Osborn, W. A.; Chinn, J.; Walker, M. L.; Scott, J. H. J.; Jones, W.; Hao, C. L.; Yao, S. H.; Wang, Z. K. How nanorough is rough enough to make a surface superhydrophobic during water condensation? *Soft Matter* **2012**, *8*, 8786−8794.
(61) Ölçeroğlu, E.; Hsieh, C.-Y.; Rahman, M. M.; Lau, K. K. S.; McCarthy, M. Full-Field Dynamic Characterization of Superhydrophobic Condensation on Biotemplated Nanostructured Surfaces. *Langmuir* **2014**, *30*, 7556−7566.
(62) Sharma, C. S.; Combe, J.; Giger, M.; Emmerich, T.; Poulikakos, D. Growth Rates and Spontaneous Navigation of Condensate Droplets Through Randomly Structured Textures. *ACS Nano* **2017**, *11*, 1673−1682.
(63) Graham, C.; Griffith, P. Drop Size Distributions and Heat-Transfer in Dropwise Condensation. *Int. J. Heat Mass Transfer* **1973**, *16*, 337−346.
(64) Xu, Z.; Zhang, L.; Wilke, K.; Wang, E. N. Multiscale Dynamic Growth and Energy Transport of Droplets during Condensation. *Langmuir* **2018**, *34*, 9085−9095.
(65) Rose, J. W. On the mechanism of dropwise condensation. *Int. J. Heat Mass Transfer* **1967**, *10*, 755−762.
(66) Dietz, C.; Rykaczewski, K.; Fedorov, A. G.; Joshi, Y. Visualization of droplet departure on a superhydrophobic surface and implications to heat transfer enhancement during dropwise condensation. *Appl. Phys. Lett.* **2010**, *97*, 033104.
(67) Wasserfall, J.; Figueiredo, P.; Kneer, R.; Rohlfs, W.; Pischke, P. Coalescence-induced droplet jumping on superhydrophobic surfaces: Effects of droplet mismatch. *Physical Review Fluids* **2017**, *2*, 123601.
(68) Chen, X.; Weibel, J. A.; Garimella, S. V. Characterization of Coalescence-Induced Droplet Jumping Height on Hierarchical Superhydrophobic Surfaces. *ACS Omega* **2017**, *2*, 2883−2890.

DOI: 10.1021/acs.langmuir.9b02232
Langmuir 2019, 35, 12858−12875

(69) Birbarah, P.; Miljkovic, N. External convective jumping-droplet condensation on a flat plate. *Int. J. Heat Mass Transfer* **2017**, *107*, 74−88.
(70) Andrieu, C.; Beysens, D. A.; Nikolayev, V. S.; Pomeau, Y. Coalescence of sessile drops. *J. Fluid Mech.* **2002**, *453*, 427−438.
(71) Adhikari, S.; Rattner, A. S. Heat transfer during condensing droplet coalescence. *Int. J. Heat Mass Transfer* **2018**, *127*, 1159−1169.
(72) Roache, P. J. Quantification of uncertainty in computational fluid dynamics. *Annu. Rev. Fluid Mech.* **1997**, *29*, 123−160.
(73) Rykaczewski, K.; Scott, J. H. J.; Fedorov, A. G. Electron beam heating effects during environmental scanning electron microscopy imaging of water condensation on superhydrophobic surfaces. *Appl. Phys. Lett.* **2011**, *98*, 093106.
(74) Rykaczewski, K.; Scott, J. H. J. Methodology for Imaging Nano-to-Microscale Water Condensation Dynamics on Complex Nanostructures. *ACS Nano* **2011**, *5*, 5962−5968.
(75) Rykaczewski, K. Microdroplet Growth Mechanism during Water Condensation on Superhydrophobic Surfaces. *Langmuir* **2012**, *28*, 7720−7729.

DOI: 10.1021/acs.langmuir.9b02232
Langmuir 2019, 35, 12858−12875